Research Article

Haofei Tian, Ganyu Li*, Jinyong Choi, Wenlou Luan, Xingtao Cui, Shen Wang, Mengqi Jin, Haotian Chen, Wenjing Chen, Xian Liang, Chengjie Zou, Liang Zhao, Sinan Han, Peijie Zou, and Xiaofei Hu

Petrogenesis and tectonic significance of the Mengjiaping beschtauite in the southern Taihang mountains

https://doi.org/10.1515/geo-2020-0324
received May 27, 2021; accepted November 22, 2021

Abstract: The evolution process of the North China Craton has been discussed by many scholars; however, the frame for the timing of the Trans-North China Block has not been fully agreed upon. Related research has mostly focused on the northern and southern sections of the Trans-North China Block, and in-depth studies on intrusive rocks in the central region are lacking. In this study, we conduct a systematic study of the petrography, the whole-rock geochemistry, and the zircon U–Pb dating for the beschtauite intrusion, located in the Mengjiaping area of the Southern Taihang Mountains. Our results demonstrate that the dyke intrusion is mainly composed of beschtauite. Laser ablation inductively coupled plasma mass spectrometry zircon U–Pb dating shows that the beschtauite intrusion occurred at ~1,880 ± 69 Ma. The beschtauite belongs to I-type granite, Arc tholeiite series, and Cale-alkaline series, with low total alkali, low potassium, and high aluminum. They are also enriched in large-ion lithophile elements, relatively depleted in high-field strength elements, and low total rare-earth elements. Based on the abovementioned data, it is suggested that the magmas for the beschtauite intrusion were metasomatized by oceanic slab subduction in the Late Paleoproterozoic. The formation time of the North China Craton basement should be set to after 1,880 Ma.

Keywords: beschtauite, I-type granite, geochemistry, Paleoproterozoic, LA-ICP-MS zircon U–Pb dating, North China Craton

* **Corresponding author: Ganyu Li,** Division of Development and Planning, Hebei GEO University, Shijiazhuang, Hebei 050031, China, e-mail: liganyuchd@163.com
Haofei Tian: Department of Oceanography, Kunsan National University, Gunsan 573-701, Republic of Korea; Institute of Resources and Environment, Hebei GEO University, Shijiazhuang, Hebei 050031, China
Jinyong Choi, Sinan Han: Department of Oceanography, Kunsan National University, Gunsan 573-701, Republic of Korea
Wenlou Luan, Xingtao Cui: Institute of Resources and Environment, Hebei GEO University, Shijiazhuang, Hebei 050031, China
Shen Wang: Airborne Survey and Remote Sensing Center of Nuclear Industry, Shijiazhuang, Hebei 50002, China
Mengqi Jin: Xi'an Center of China Geological Survey, China Geological Survey, Xi'an 710054, China
Haotian Chen: Department of Software Convergence Engineering, Kunsan National University, Gunsan 54150, Republic of Korea; College of Information and Engineering, Hebei GEO University, Shijiazhuang 50031, China
Wenjing Chen: Institute of Environment-Geo Survey of Hebei Provincial Bureau of Coal Geology, Shijiazhuang, Hebei 050051, China
Xian Liang: Ore Deposit and Exploration Centre, School of Resources and Environmental Engineering, Hefei University of Technology, Hefei 230009, China
Chengjie Zou: College of Earth Sciences, Chengdu University of Technology, Chengdu 610059, China
Liang Zhao: College of Energy, Chengdu University of Technology, Chengdu 610059, China
Peijie Zou: Department of Chinese Language and Literature, Kunsan National University, Gunsan 573-701, Republic of Korea
Xiaofei Hu: Department of Physical Education, Kunsan National University, Gunsan 573-701, Republic of Korea

1 Introduction

The North China Craton is one of the oldest cratons in the world [1]. Compared with other cratons worldwide, the North China Craton has recorded almost all major tectonic events after 3.5 Ga during the early development of the Earth despite possessing a limited exposed area [2]. This craton exhibits a dual paleostructural geographic pattern comprising an early Precambrian metamorphic crystalline basement and a Mesoproterozoic sedimentary cap [3]. Several geologists have explored the structural complexity and multistage tectonic evolution of the North China Craton [4–15].

Currently, research on the North China Craton mainly focuses on six aspects as follows: the number of tectonic

units, formation mechanism, integration age, tectonic boundary, collision mode, and subduction polarity [16–30]. Several geologists have studied the formation and tectonic evolution of the early Precambrian metamorphic crystalline basement of the North China Craton and proposed different basement-division schemes [31–46]. The tripartite scheme of the Eastern Block, Western Block, and Trans-North China Block, proposed by Zhao et al. [4–6], is one of the widely accepted schemes (Figure 1). The findings associated with the formation mechanism and formation age of the North China Craton basement are controversial, particularly the final formation age of the Precambrian basement, showing conflicting results of 2,500 and 1,900–1,800 Ma [17–21,30,32–45]. The formation mechanism and formation age of the Trans-North China Block of the North China Craton are critical to comprehensively understand the formation history of the North China Craton basement. Additionally, related studies have mostly focused on the northern and southern sections of the Trans-North China Block [10,47–68], and there is a lack of in-depth studies on intrusive rocks in the central region [18,69–75].

The study area is located in the eastern part of the central Trans-North China Block of the North China Craton. A large number of dykes are intruded in the study area. Previous studies have identified the dykes as quartz augite porphyry. After electron microprobe analysis of the dyke samples, we redesignated the dykes as beschtauite. Previous studies have shown that the petrogenesis types of beschtauite are I-type granite [76–80], A-type granite [81–85], and adakite [79,86–89]. Beschtauite occurs in both subduction [77,90–93] and extensional settings [76,81,82,94,95]. The beschtauite in the study area is poorly studied, and its petrogenesis and tectonic setting still need to be studied in depth.

The beschtauite in the Mengjiaping area of the southern section of the Taihang Mountains is selected as the research area in this study. Through detailed geological fieldwork, laboratory petrographic study, geochemical analysis, and zircon U–Pb chronology research, we will discuss the formation period, petrogenesis, and tectonic setting, aiming to provide geological evidence for the tectonic evolution of the North China Craton.

2 Geological setting

The Mengjiaping area is located in the eastern part of the central Trans-North China Block, which is located in the southern section of the Taihang Mountains. It is distributed in western Neiqiu County, Xingtai City, Hebei Province. The Nansizhang and Nansi formations of the Gantaohe Group are the main strata in this area, wherein the relationship between the Nansizhang and Nansi formations is a conformable contact. The lithology of the lower section of the Nansizhang formation mainly comprises metamorphic conglomerates, meta-arkosic sandstones, and slate. By contrast, the upper section mainly comprises chlorite schist with metamorphic feldspar sandstone, metabasalt, tuff

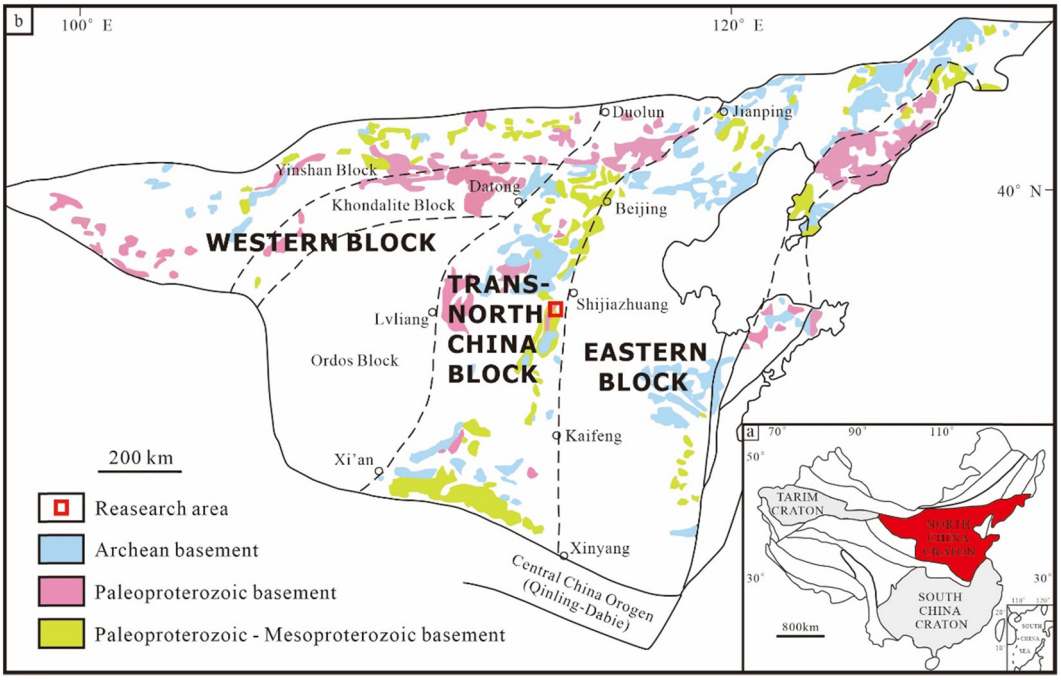

Figure 1: Structural model of the North China Craton basement [6].

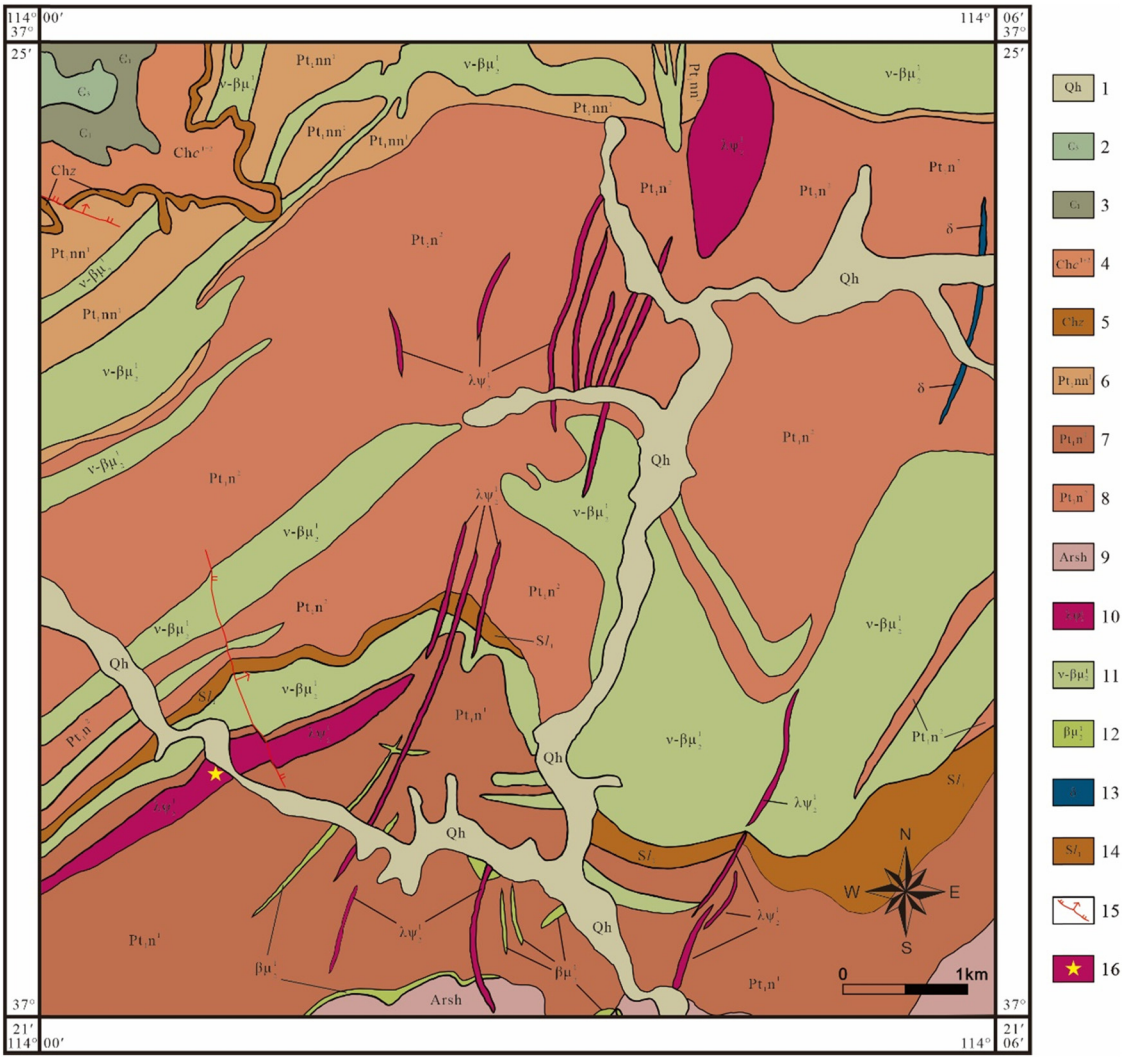

Figure 2: Geological map of Mengjiaping in the southern Taihang Mountains (taken from the 1:50,000 Motianling map [99]). (1) Loess, sand, and gravel, (2) upper cambrian, (3) lower cambrian, (4) Changzhougou formation, (5) Zhaojiazhuang formation, (6) Section 1 of Nansi formation, (7) Section 1 of Nansizhang formation, (8) Section 2 of Nansizhang formation, (9) Shijialan formation, (10) beschtauite, (11) gabbro diabase, (12) diabase, (13) diorite dyke, (14) slate, (15) normal fault, and (16) sampling location.

lava, and thin-bedded amphibolite schist. The Nansi formation mainly comprises metabasalt, quartzose arkose, metamorphic feldspar sandstone, dolomite, and slate [96]. Magmatic rocks are widely distributed in the Nansi formation (2,090 Ma) and Nansizhang formation (2,087–2,090 Ma) [22,100], and the main types of intrusive rocks include diabase (2,090 Ma) [30,97], beschtauite (1,880 Ma), and a small amount of diorite. The beschtauite is produced in dykes, possessing a length and width of 20–4,500 and 2–35 m, respectively. The dykes are mainly oriented northeast–southwest, followed by the near-south–north direction. The contact boundary between the intrusive and surrounding rocks is prominent and almost straight; the dykes often interpenetrate the surrounding rocks (Figures 2 and 3a). Diabase xenoliths are found at the contacts between the dykes and the surrounding rocks. The number of xenoliths tends to decrease from the outside to the inside of the dyke. The effect of metamorphic deformation on the rock is weak, which is the result of the flow-like arrangement of sheet minerals. The beschtauite is gray, possessing a porphyritic texture and a block structure (Figure 3b and c). The phenocrysts are mainly comprises K-feldspar (10–15%), plagioclase (15–20%), quartz (50–55%), and biotite (3–5%; Figure 3d and e). Among them, most quartz phenocrysts are round and granular. K-feldspar develops according to the Carlsbad twin law, mainly orthoclase. Some K-feldspar phenocrysts occur as giant phenocrysts with a size of 0.5–1.5 cm. The plagioclase exhibits polysynthetic twinning,

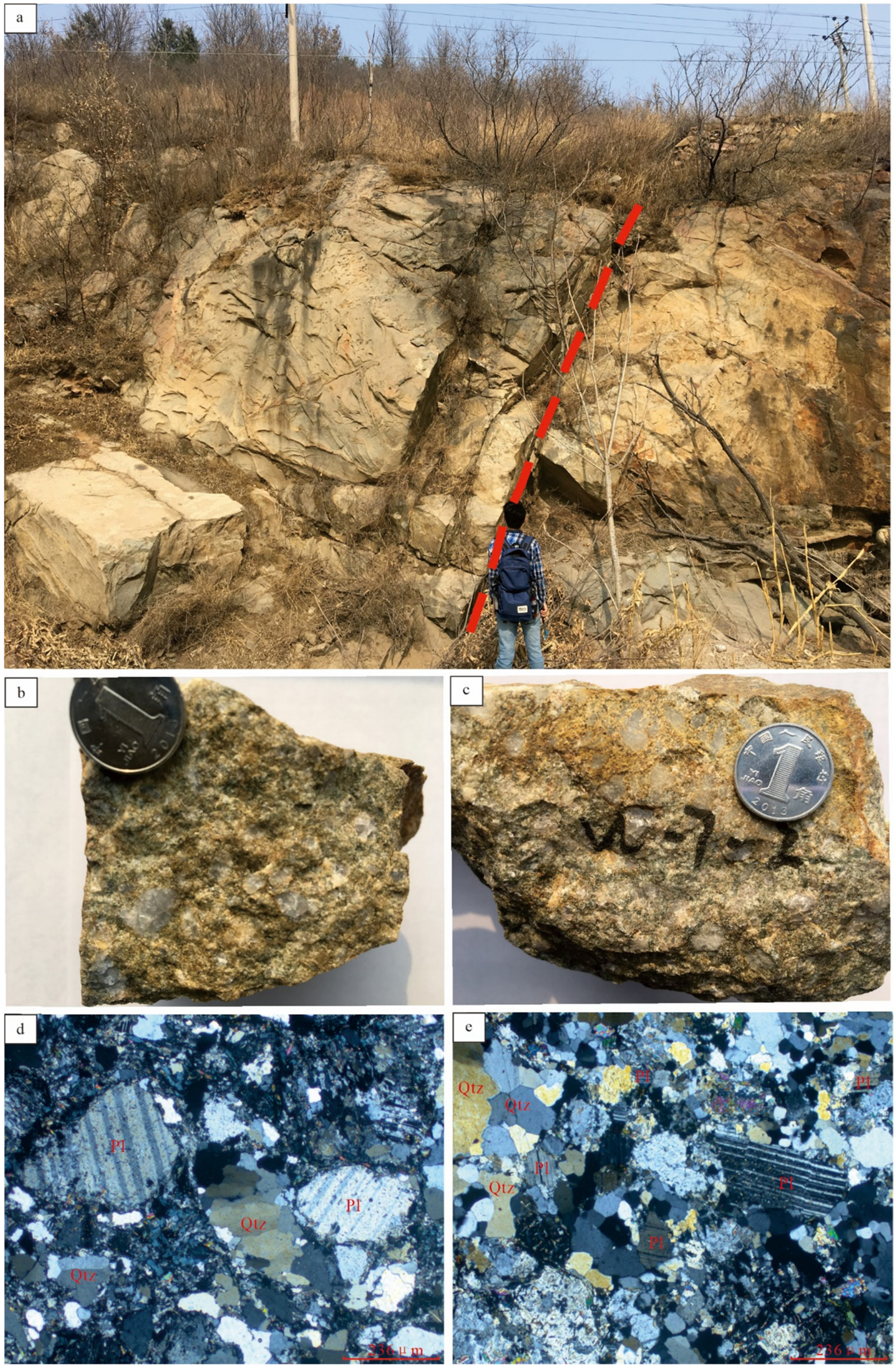

Figure 3: Field photographs and lithologic photographs in Mengjiaping; Qtz – quartz and Pl – plagioclase. (a) Rock mass photos, (b,c) Rock specimen photos, (d), (e) Microscopic photos of rock flakes.

Table 1: U–Pb isotopic testing data of the beschtauite in Mengjiaping

Sample no.	Content (μg/g)		Th/U	$n(^{207}Pb)/n(^{206}Pb)$		$n(^{207}Pb)/n(^{235}U)$		$n(^{206}Pb)/n(^{238}U)$		$n(^{208}Pb)/n(^{232}Th)$		$^{207}Pb/^{235}U$ Age (Ma)		$^{206}Pb/^{238}U$ Age (Ma)		$^{208}Pb/^{232}Th$ Age (Ma)		pr
	^{232}Th	^{238}U		Test	1σ	Test	1σ	Test	1σ	Test	1σ	Test	1σ	Test	1σ	Test	1σ	
LF01	74.58	134.25	0.58	0.1369	0.0007	9.5457	0.1406	0.5050	0.0079	0.1140	0.0038	2,392	14	2,635	34	2,181	69	0.9
LF02	102.23	314.39	0.35	0.1283	0.0005	8.5065	0.1143	0.4794	0.0061	0.1114	0.0028	2,287	12	2,525	27	2,134	52	0.9
LF03	138.47	252.86	0.56	0.1353	0.0007	8.5489	0.1585	0.4582	0.0094	0.0929	0.0030	2,291	17	2,432	41	1,796	56	0.9
LF04	67.27	167.34	0.45	0.1237	0.0005	9.1183	0.1305	0.5327	0.0066	0.1162	0.0027	2,350	13	2,753	28	2,222	49	0.8
LF05	210.14	484.49	0.48	0.1148	0.0008	5.0794	0.1035	0.3197	0.0045	0.0678	0.0011	1,833	17	1,788	22	1,326	21	0.9
LF06	242.79	512.76	0.51	0.1177	0.0004	4.9320	0.1125	0.3029	0.0046	0.0635	0.0014	1,808	19	1,706	23	1,244	27	0.9
LF07	32.36	94.01	0.37	0.1275	0.0006	9.7532	0.1728	0.5529	0.0047	0.1335	0.0042	2,412	16	2,837	20	2,534	75	0.8
LF08	85.04	219.28	0.41	0.1229	0.0007	7.7755	0.0997	0.4582	0.0045	0.1053	0.0023	2,205	12	2,431	20	2,023	42	0.9
LF09	60.10	130.09	0.46	0.1382	0.0017	9.7568	0.1775	0.5102	0.0057	0.1250	0.0037	2,412	17	2,658	24	2,381	67	0.9
LF10	103.28	376.67	0.27	0.1128	0.0017	5.1293	0.1106	0.3285	0.0041	0.0906	0.0077	1,841	18	1,831	20	1,752	144	0.9
LF11	122.71	370.16	0.34	0.1161	0.0006	5.4593	0.1353	0.3404	0.0081	0.0859	0.0027	1,894	21	1,889	39	1,665	50	0.9
LF12	59.41	163.89	0.38	0.1288	0.0008	9.6886	0.1086	0.5448	0.0043	0.1295	0.0031	2,406	10	2,803	18	2,461	56	0.8
LF13	76.15	210.74	0.38	0.1241	0.0007	7.8117	0.1840	0.4561	0.0105	0.1185	0.0037	2,210	21	2,422	47	2,263	68	0.9
LF14	82.79	349.73	0.21	0.1070	0.0006	5.9130	0.2161	0.4000	0.0143	0.0850	0.0049	1,963	32	2,169	66	1,650	91	0.9
LF15	121.99	433.92	0.30	0.1079	0.0004	4.6789	0.0907	0.3145	0.0061	0.0516	0.0015	1,763	16	1,763	30	1,017	29	0.9

mainly albite. The matrix comprises fine-granular and occasionally cryptocrystalline orthoclase, albite, quartz, mica, and chlorite. The macrophyllite typically exhibits a flow-like arrangement of sheet minerals, sometimes exhibiting the visible potassium metasomatism phenomenon. The edges of microcline or microstripe feldspar exhibit a visible carbonate metasomatism.

3 Methods

The sampling coordinates of the zircon U–Pb dating sample (35 kg) were 37°22′36″ N and 114°7′8″ E. The zircon samples were crushed in the Laboratory of the Langfang Institute of Regional Geology and Mineral Survey, Hebei Province. The zircon samples were placed in an epoxy resin, and they were abrasively polished until the zircon core was exposed. The internal structure of zircon was observed using cathodoluminescence (CL) microphotography by combining the reflected and transmitted lights. Microfield measurements for the *in situ* zircon U–Pb dating samples were performed at the Key Laboratory of Xi'an Center of Geological Survey, via LA-ICP-MS (Agilent 7500X). A Geolas Pro laser with a laser spot diameter of 32 μm, a laser energy density of 6.0 J/cm^2, and a laser frequency of 9 Hz was used. Helium was used as the carrier gas to remove the denuded materials. Zircon 91500 and NIST610 were used as external and internal standards, respectively, for the U–Th–Pb isotope analysis. For principles and a detailed analysis process of the U–Th–Pb isotope analysis, refer to the Yuan et al. [100]. The experimental data containing the isotopic ratios were calibrated using the method proposed by Andersen [101] to minimize the influence of ordinary Pb on the test results. Using the $^{206}Pb/^{238}U$ ratio, the error of the weighted mean was calculated as 2σ. The ICP-MS Data Cal 8.3 program was used for data processing, and Isoplot (Version 4.0) was used for calculating the weighted age and obtaining the harmonic plot [102].

The total weight of the 12 beschtauite samples is 4 kg. The samples were collected near the highway in the Mengjiaping village and were used for the geochemical analysis. The beschtauite samples were fresh, and their alteration was weak. The beschtauites were cleaned, dried, and smashed to 200-mesh particles. They were analyzed using the wet chemical method at the Key Laboratory of Hebei GEO University. The major elements were analyzed using a ZSX Primus α X-ray fluorescence spectrometer. The trace and rare-earth (rare-earth elements [REEs]) elements were analyzed using MS and ICP atomic emission MS.

4 Results

4.1 Zircon U–Pb dating

Table 1 presents the 12 data obtained from the LA-ICP-MS zircon U–Pb dating. The zircon CL image (Figure 4) indicates that most zircon samples showed intact crystal structure with clear edges and faces, and their long axes were between 150 and 280 μm. Their aspect ratio was between 1:1 and 3:1. The zircon particles exhibited a complete crystal structure, and both cylindrical and conical surfaces could be observed. All the zircon particles exhibited clear oscillating growth zones in the CL images, and some zircon particles exhibited round central nuclei. The Th/U ranged from 0.21 to 0.58 (>0.1), indicating the magmatic zircon characteristics of the sample [103]. The weighted age was 1,880 ± 69 Ma (MSWD = 1.17, N = 12; Figure 5).

5 Petrogeochemical characteristics

5.1 Major elements

The major elemental contents and related parameters of the beschtauite samples are shown in Table 2. The SiO_2 content ranged from 71.1 to 77.4%, with an average of 75.2%. The Al_2O_3 content was high, ranging from 11.75 to 15.3%, with an average of 13.65%. The $Fe_2O_3^T$ content ranged from 1.30 to 3.94%, with an average of 2.52%. The MgO content was 0.48–1.76%. The total alkali content ($K_2O + Na_2O$) ranged from 4.73 to 6.04%, with an average of 5.53%. The K_2O content was 0.70–2.53%, with an average of 1.53%. The Na_2O/K_2O ratio ranged from 1.35 to 6.87, with an average of 3.13, which places this sample in the sodium type. In the volcanic rock TAS classification diagram, all the samples fall into the granite region (Figure 6a). The K_2O/SiO_2 ratio ranged from 0.01 to

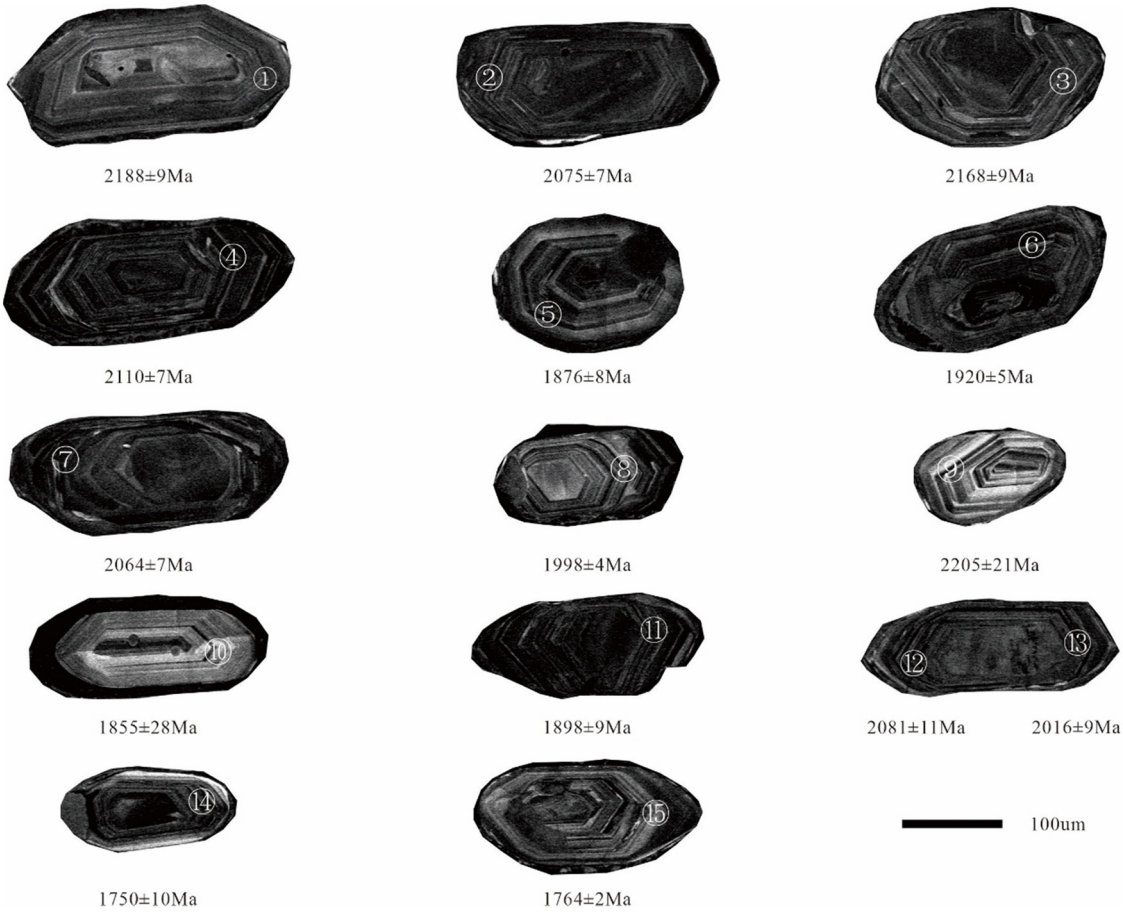

Figure 4: Zircon CL images of the beschtauite in Mengjiaping.

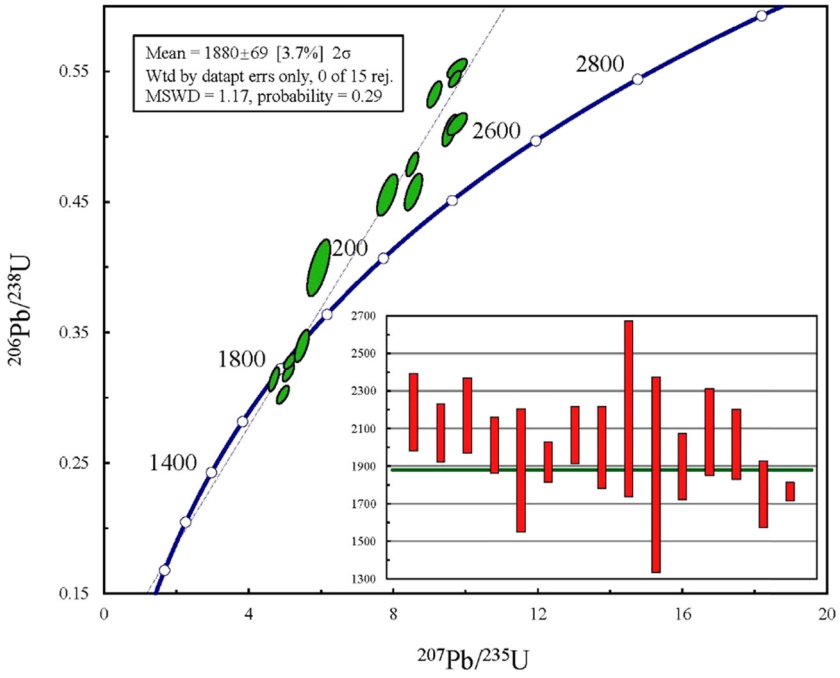

Figure 5: Zircon U–Pb age concordance and weighted mean age of the beschtauite in Mengjiaping.

0.03, with an average of 0.02. Moreover, the alkalinity ratio (AR) ranged from 1.95 to 2.52. The diagram of the AR–SiO_2 and SiO_2–K_2O shows that the beschtauite belongs to the low-potassium series and the calc-alkaline series (Figure 6b and c). The saturation (A/CNK) ranged from 1.17 to 1.79, with an average of 1.47. In the A/CNK–A/NK diagram, all samples are peraluminous granite (Figure 6d).

5.2 Trace and REEs

Based on the primitive mantle-normalized multielement spider diagram (Figure 7a), the elemental distribution characteristics of the granite samples were generally consistent. Compared with the Earth's crust, the high-field strength elements (HFSEs), such as P, Nb, Ce, Ta, Sr, and Ti, were relatively depleted, whereas the large-ion lithophile elements (LILEs), such as Rb, Th, and K, were relatively enriched, which is a characteristic of a volcanic-arc granite. The normalized REE partition pattern diagram of chondrites revealed a right-leaning pattern of enriched LREE and depleted HREE (Figure 7b). The LREE/HREE ratio was 9.69–18.69, and the $(La/Yb)_N$ ratio was 13.55–33.47, which were considerably larger than 1; the fractionation of LREEs and HREEs was obvious. The $(La/Sm)_N$ ratio was 3.60–6.56, and the $(Gd/Yb)_N$ ratio was 2.38–3.29. A weak HREE differentiation was observed, a weak Eu negative anomaly was found (δEu = 0.74–1.11), and Ce showed no obvious positive or negative anomaly (δCe = 0.87–1.00).

6 Discussion

6.1 Formation era

From bottom to top, the strata of the Gantaohe Group include the Nansizhang, Nansi, Songting, and Niushan formations. The Mengjiaping beschtauite mainly intrudes the strata of the Nansizhang formation and to a lesser extent in the Nansi formation. Previous studies showed that the age of rhyolite in the upper part of the Nansizhang formation is 2,088 ± 8 Ma [98], the age of metamorphic basalt in the Nansizhang formation is 2,087 ± 16 Ma [20], the age of diabase in the Nansizhang formation is 2,090 ± 14 Ma [97], and the age of dolomite in the Nansi formation is 2,090 ± 3 Ma [97]. The LA-ICP-MS zircon U–Pb age of the beschtauite obtained in the present study is 1,880 ± 69 Ma, which is less than the age of the Nansizhang and Nansi formations and consistent with geological facts. Therefore, it can be deduced that the magma emplacement age is 1,880 ± 69 Ma, and the emplacement era is during the Late Paleoproterozoic.

Table 2: Major elements (wt%), trace elements (10^{-6}), REEs, and related parameters of the beschtauite in Mengjiaping

Sample no.	w-1	w-2	w-3	w-4	w-5	w-6	w-7-1	w-7-2	w-8	w-9	w-10	w-11
SiO_2	76.8	73.2	74.9	77.4	73.2	73.5	77.1	77.3	71.1	76.0	75.2	76.9
TiO_2	0.18	0.30	0.26	0.18	0.26	0.37	0.17	0.15	0.33	0.16	0.18	0.17
Al_2O_3	13.0	13.9	14.1	12.74	12.96	15.9	11.88	11.75	15.3	13.91	15.18	13.20
$Fe_2O_3^T$	1.87	3.06	2.37	1.88	3.18	1.30	2.46	2.72	3.94	2.54	2.51	2.44
MnO	0.041	0.053	0.047	0.036	0.043	0.013	0.049	0.049	0.037	0.048	0.042	0.040
MgO	0.67	1.18	1.06	0.70	0.75	0.48	1.11	1.22	1.76	1.07	1.25	1.07
CaO	0.74	0.51	0.69	0.56	1.52	0.79	0.39	0.33	0.68	0.36	0.44	0.41
Na_2O	4.78	3.87	3.88	4.27	3.41	3.49	4.06	4.05	4.29	4.09	4.02	3.74
K_2O	0.70	2.17	2.05	1.39	2.53	2.46	1.13	1.17	1.68	1.09	1.00	0.99
P_2O_5	0.079	0.088	0.062	0.042	0.043	0.088	0.069	0.051	0.072	0.048	0.052	0.048
COL	0.59	1.07	0.9	0.72	1.51	1.25	1.90	0.74	1.38	0.73	0.76	0.65
TOTAL	99.45	99.40	100.32	99.92	99.41	99.64	100.32	99.53	100.57	100.05	100.63	99.66
Na_2O/K_2O	6.87	1.78	1.89	3.07	1.35	1.42	3.58	3.46	2.55	3.74	4.03	3.78
K_2O/SiO_2	0.01	0.03	0.03	0.02	0.03	0.03	0.01	0.02	0.02	0.01	0.01	0.01
A/CNK	1.30	1.44	1.43	1.33	1.17	1.61	1.38	1.38	1.51	1.62	1.79	1.66
A/NK	1.51	1.59	1.64	1.49	1.55	1.89	1.50	1.48	1.72	1.76	1.97	1.83
AR	2.33	2.44	2.34	2.48	2.39	2.11	2.47	2.52	2.19	2.14	1.95	2.07
$Mg^{\#}$	45.75	47.58	51.28	46.70	35.69	46.49	51.50	51.35	51.25	49.78	53.96	50.79
Rb	20.4	50.2	43.2	33.2	42.0	39.6	26.4	38.7	45.4	25.2	21.7	20.1
Ba	258	481	580	505	682	997	182	273	470	205	187	180
Th	5.62	9.58	8.10	5.33	9.56	12.0	6.62	5.53	6.32	7.21	7.40	7.33
U	0.499	0.747	0.718	0.510	1.24	0.691	0.543	0.465	0.800	0.651	0.623	0.694
Ta	0.38	0.48	0.33	0.27	0.31	0.51	0.19	0.16	0.40	0.18	0.19	0.23
Nb	3.97	5.05	4.10	3.21	3.71	6.82	2.20	1.90	5.66	2.32	2.36	2.28
La	22.20	27.70	19.50	16.50	25.20	13.60	20.40	17.10	29.90	14.50	20.10	16.90
Ce	41.80	54.90	35.40	31.30	46.20	25.40	36.50	28.70	58.40	27.40	36.00	31.00
Pb	13.10	10.80	9.07	10.80	23.80	7.25	6.97	6.89	6.40	6.12	6.93	6.32
Pr	5.11	5.97	4.10	3.46	4.96	3.12	4.20	3.33	6.38	3.29	4.06	3.62
Sr	128	94.7	96.4	151	88.9	103	98.6	108	126	97.2	122	106
Nd	18.6	20.1	14.0	12.2	16.8	12.0	14.1	11.4	22.3	11.9	13.9	12.9
Zr	41.8	64.0	66.0	35.7	52.2	47.8	47.5	41.8	54.3	57.4	51.4	40.8
Hf	1.11	1.71	1.67	0.93	1.47	1.33	1.36	1.21	1.38	1.55	1.36	1.13
Sm	3.29	3.11	2.06	2.02	2.48	2.44	2.18	1.74	3.51	2.08	2.09	2.06
Eu	0.89	0.73	0.56	0.65	0.71	0.84	0.55	0.52	1.07	0.50	0.53	0.50
Y	9.52	9.27	5.74	5.20	5.98	7.19	5.76	3.61	10.4	5.24	5.17	5.10
Gd	2.88	2.80	1.77	1.70	2.15	2.07	1.88	1.48	3.14	1.73	1.78	1.75
Tb	0.34	0.32	0.19	0.18	0.22	0.25	0.20	0.16	0.33	0.19	0.19	0.19
Dy	1.99	1.89	1.07	1.04	1.18	1.53	1.15	0.87	1.90	1.07	1.05	1.04
Ho	0.37	0.36	0.20	0.19	0.21	0.28	0.21	0.16	0.36	0.20	0.19	0.19
Er	1.15	1.16	0.70	0.62	0.68	0.87	0.68	0.50	1.15	0.61	0.62	0.60
Tm	0.15	0.16	0.096	0.084	0.090	0.12	0.088	0.065	0.15	0.080	0.083	0.079
Yb	0.88	0.96	0.61	0.52	0.54	0.72	0.55	0.39	0.93	0.48	0.50	0.47
Lu	0.13	0.14	0.094	0.081	0.082	0.11	0.082	0.057	0.14	0.075	0.075	0.072
ΣREE	99.71	120.35	80.37	70.53	101.49	63.44	82.81	66.44	129.66	64.18	81.18	71.40
LREE	91.82	112.56	75.65	66.12	96.34	57.50	77.97	62.76	121.56	59.75	76.69	67.02
HREE	7.89	7.79	4.72	4.41	5.15	5.93	4.84	3.68	8.09	4.43	4.50	4.38
LREE/HREE	11.64	14.45	16.03	14.98	18.69	9.69	16.11	17.03	15.02	13.48	17.06	15.29
δEu	0.86	0.74	0.88	1.05	0.92	1.11	0.80	0.97	0.96	0.78	0.82	0.79
δCe	0.93	1.00	0.92	0.97	0.95	0.92	0.92	0.87	0.99	0.93	0.92	0.93
$(La/Sm)_N$	4.36	5.75	6.11	5.27	6.56	3.60	6.04	6.34	5.50	4.50	6.21	5.30
$(La/Yb)_N$	18.10	20.70	22.93	22.76	33.47	13.55	26.61	31.45	23.06	21.67	28.84	25.79
$(Gd/Yb)_N$	2.71	2.41	2.40	2.70	3.29	2.38	2.83	3.14	2.79	2.98	2.95	3.08
Rb/Sr	0.16	0.53	0.45	0.22	0.47	0.39	0.27	0.36	0.36	0.26	0.18	0.19
Rb/Nb	5.14	9.95	10.53	10.35	11.32	5.81	11.98	20.38	8.02	10.85	9.19	8.80
La/Nb	5.59	5.49	4.76	5.14	6.79	1.99	9.27	9.00	5.28	6.25	8.52	7.41
La/Yb	25.23	28.85	31.97	31.73	46.67	18.89	37.09	43.85	32.15	30.21	40.20	35.96

(*Continued*)

Table 2: *Continued*

Sample no.	w-1	w-2	w-3	w-4	w-5	w-6	w-7-1	w-7-2	w-8	w-9	w-10	w-11
K/Rb	0.034	0.043	0.048	0.042	0.060	0.062	0.043	0.030	0.037	0.043	0.046	0.049
Sr/Y	13.40	10.21	16.80	29.07	14.87	14.29	17.11	29.83	12.13	18.53	23.51	20.78
Sr/Nd	6.85	4.70	6.89	12.43	5.28	8.54	6.97	9.47	5.66	8.17	8.74	8.18
Zr/Hf	37.63	37.40	39.58	38.54	35.42	35.85	34.85	34.52	39.32	36.98	37.84	36.10
Nb/Ta	10.58	10.56	12.37	11.89	11.97	13.36	11.54	12.24	14.04	12.91	12.20	10.06

A/CNK = $(Al_2O_3)/[(CaO) + (Na_2O) + (K_2O)]$; $Mg^{\#} = 100 \times [(MgO)/40.3044]/[(MgO)/40.3044 + (FeO^T)/71.844]$; A/NK = $(Al_2O_3)/[(Na_2O) + (K_2O)]$; AR = $[(Al_2O_3) + (CaO) + (Na_2O) + (K_2O)]/\{(Al_2O_3) + (CaO) - [(Na_2O) + (K_2O)]\}$; $FeO^T = Fe_2O_3^T \times 0.8998 \times 0.85$; $\delta Eu = Eu_N/(Sm_N \times Gd_N)^{1/2}$; $\delta Ce = Ce_N/(La_N \times Pr_N)^{1/2}$; and the subscript N denotes standardization with chondrites [107].
$Mg^{\#}$ reflects the ratio of magnesium to iron in the rock.

6.2 Petrogenesis

The major element contents of beschtauite include high Si (71.1–77.4%), low alkali (K_2O = 0.70–2.53%, Na_2O = 3.41–4.78%), and high aluminum saturation index (A/CNK: 1.17–1.79%). It also has the characteristics of low P (0.04–0.08%), low Mg (0.48–1.76%), and low Ti (0.15–0.37%). Among the trace elements, europium and cerium do not have obvious anomalies (δEu = 0.74–1.11, δCe = 0.87–1.00). The beschtauite is enriched in LILEs such as Rb and relatively deficient in HFSEs such as Nb. These factors provide beschtauite the Si-rich and P-poor characteristics of A-type granite; similarities

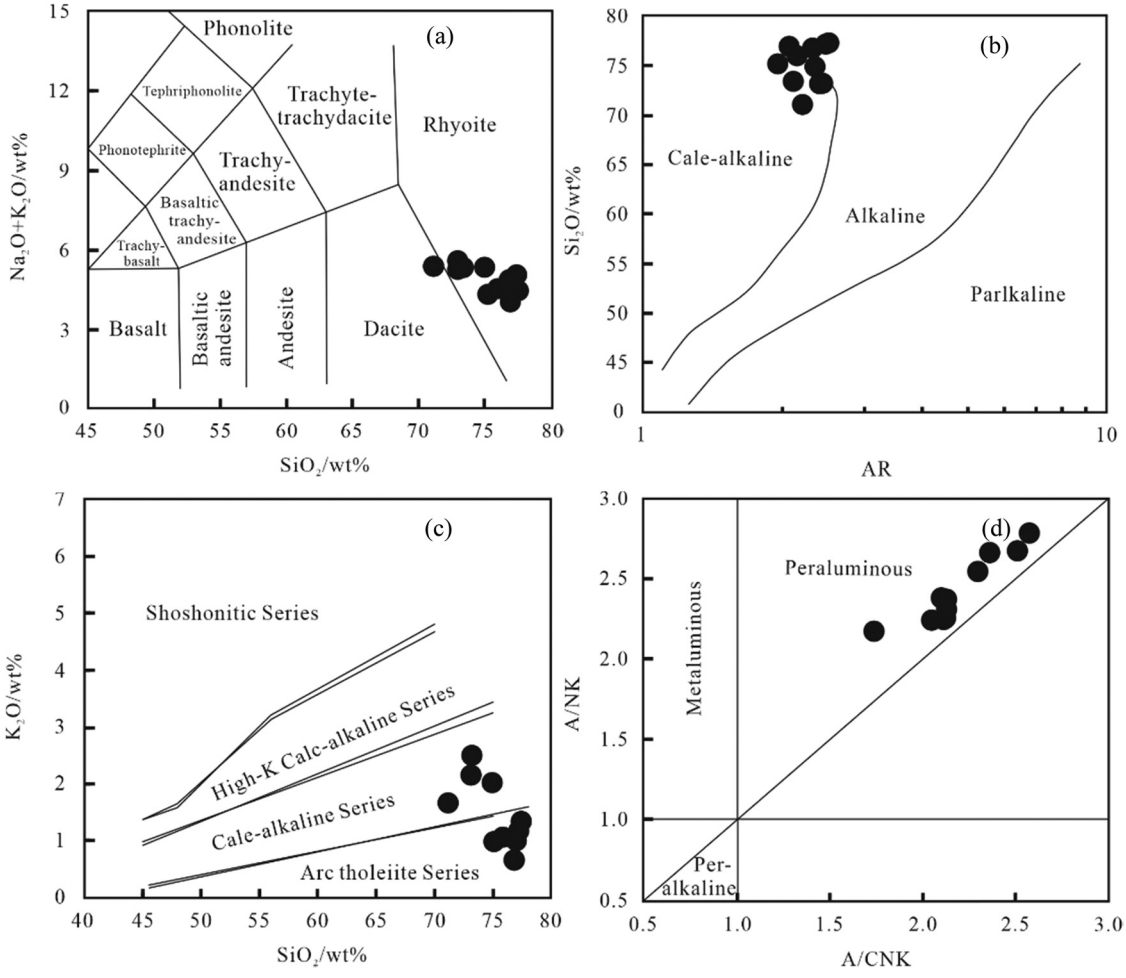

Figure 6: (a) Diagram of $Na_2O + K_2O$–SiO_2 (TAS) in granitoids [104], (b) AR-SiO_2 diagram [105], (c) K_2O–SiO_2 diagram [105], and (d) A/NK–A/KNC diagram [106].

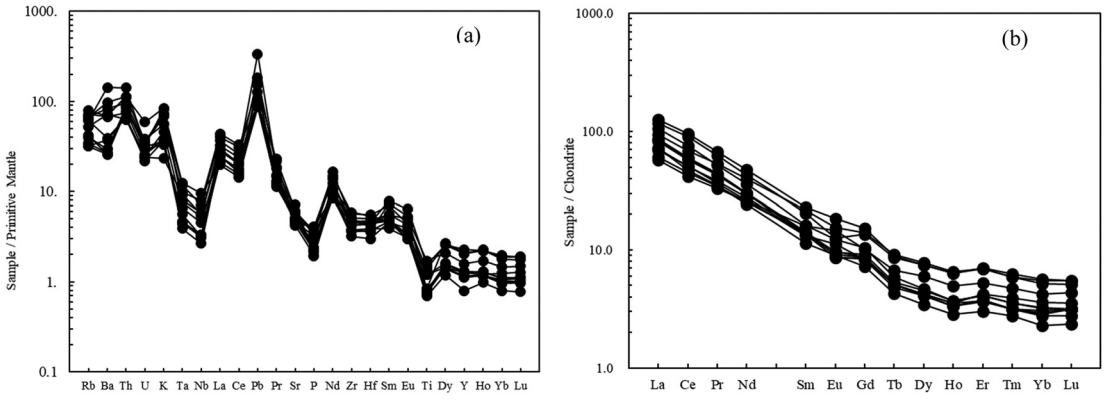

Figure 7: (a) Primitive mantle-normalized multielement spider diagram and (b) chondrite-normalized REE patterns [107].

to high Si, peraluminous S-type granite, and the Na-rich characteristics of I-type granite. Therefore, the petrogenetic type of beschtauite is worth discussing.

Granite is an important component of the continental crust. It can be divided into I-type, S-type, and A-type based on the characteristics of the magma source area [108–111]. Among these granites, A-type granites, usually contain signature alkaline dark minerals such as riebeckite–arfvedsonite, aegirine–augite, and fayalite [112]. In terms of geochemical composition, they are usually Si rich, K rich, Ga rich, Zr rich, Nb rich, Ta rich, and HFSE rich as well as possessing high diagenetic temperatures, which make them high-temperature granites [111,113,114]. No typical A-type granite minerals were observed in the beschtauite thin sections. Beschtauite trace elements have lower Ga, Zr, Nb, and other HFSEs. Herein, the geochemical characteristics of the beschtauite show that the ranges of 10,000 Ga/Al (2.57–1.48) and Zr + Nb + Ce + Y (75×10^{-6} to 133×10^{-6}) are significantly lower than the lower limits of 3.75 and 350×10^{-6} proposed for A-type granite. Simultaneously, in the granite classification diagram (Figure 8a–d), all the rock samples fall into the region of non-A-type granites. Hence, it can be concluded that the beschtauite is more likely to be an I-type or S-type granite with high differentiation, not an A-type granite.

Divergent I- or S-type granites tend to have similar major element characteristics and mineral assemblages. Their petrogenetic types are difficult to identify accurately [115]. However, Pichavant et al. showed that phosphorus has a high solubility in strongly peraluminous melts, and the content increases with increasing fractionation [116]. In contrast, phosphorus has a very low solubility in aluminous or weakly peraluminous melts, and the content decreases with the increase of the degree of differentiation. The relationship between P_2O_5 and SiO_2 can be used as an effective discriminator under the premise that the evolved samples belong to the same rock suite. The P_2O_5 content in beschtauite was low, and the contents of P_2O_5, TiO_2, and $Fe_2O_3^T$ decreased with increasing SiO_2 contents (Figure 9a, c, and d). This does not conform to the typical characteristic that apatite increases with an increase in the SiO_2 content in S-type granites. The beschtauite source area is presumed to be peraluminous or weakly peraluminous. The beschtauite has high Na_2O (>3.41%), which differs significantly from typical S-type granite features [110,112]. Mineralogically, the typical S-type granite aluminum-rich minerals such as corundum, tourmaline, cordierite, and garnet are not found [117]. In addition, beschtauite has a well-defined ring zone of nascent zircons compared to the highly differentiated pale granites while clearly differing from the geochemical characteristics and classification of pale granites [118,119]. To summarize, the beschtauite in the Mengjiaping area is a highly differentiated I-type granite.

Three main petrogenesis types of I-types granite are indicated by previous data. The first type is the partial melting and crystallization of the mantle-derived magma [123]. The second type is the mantle-derived differentiated basic magma that penetrates the lower crust and mixes with the crust-derived felsic magma to form a mixed magma chamber in the shallow source, which was formed by separation and crystallization in the later stage of temperature drop [108,124]. The third type is the partial melting of crustal materials owing to the invasion of the magma with mantle differentiation at the bottom to form highly differentiated I-type granite [126,127].

The magma formed via the partial melting or separation crystallization of the mantle is basic or neutral and must exhibit a low SiO_2 content and high $Mg^{\#}$ [128]. The beschtauite shows a high SiO_2 content within a small range (71.1–77.4%), lacking the separation

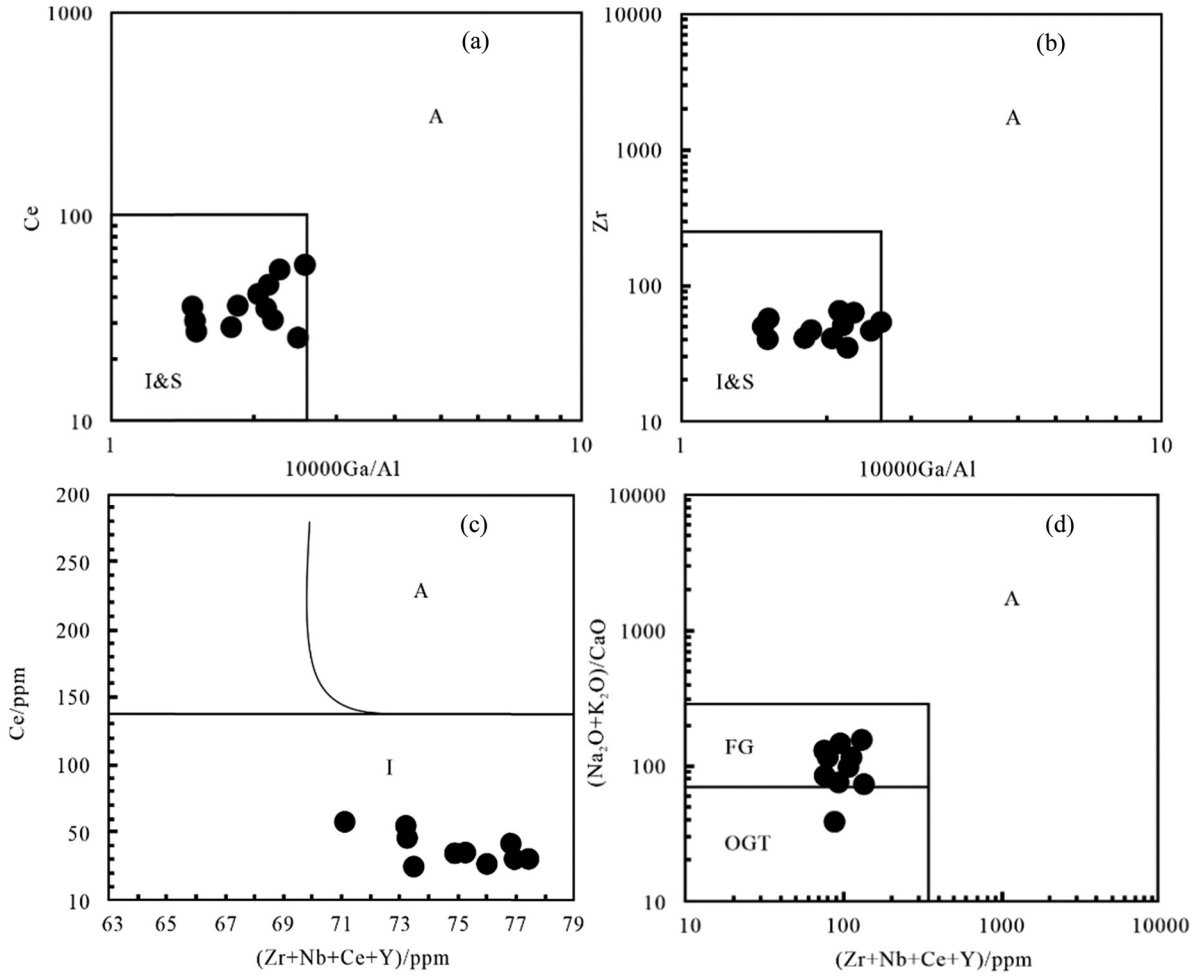

Figure 8: (a) 10,000 Ga/Al–Ce diagram [121], (b) 10,000 Ga/Al–Zr diagram [121], (c) SiO_2–Ce diagram [121], and (d) (Zr + Nb + Ce + Y)–(Na_2O + K_2O)/CaO diagram [120].

sequence from basalt to granodiorite and then to granite. Moreover, it exhibits a low $Mg^{\#}$ (35.69–53.96), indicating that the magma source area of the beschtauite in Mengjiaping cannot be directly derived from the partial melting and separation crystallization of the mantle-derived magma. The Rb/Nb ratio is 5.14–20.38, with an average of 10.19, and the Sr/Y ratio is 10.21–29.83, with an average of 18.38. Furthermore, the Nb/Ta ratio is 10.06–14.04, with an average of 11.98, close to that of the crustal average (12.22) [105,106] and lower than that of the original mantle average (17.4) [102], indicating the presence of continental crustal materials. The Zr/Hf ratio is 34.52–39.58, with an average of 37.00, higher than that of the original mantle average (36.25) [105] and higher than that of the crustal average (35.5) [105,129], reflecting the obvious fractionation during magmatic evolution. The Rb/Sr ratio is 0.16–0.53, with an average of 0.32, which is consistent with that of the global upper crustal average (0.32) [105]. These characteristics are more inclined to the third-type petrogenesis of I-type granites. Owing to the underplating of mantle-derived magma in this petrogenesis, the crustal material was partially melted, and the beschtauite in Mengjiaping was formed.

Melts formed under high pressures will exhibit a higher $(Al_2O_3)/(Fe_2O_3 + MgO + TiO_2)$ ratio than those formed under low pressures. The crust–mantle interaction occurs in the region between the high-pressure and low-pressure curves. This region occurs in the depth range of the crust–mantle interaction processes [122]. The $(Al_2O_3)/(Fe_2O_3 + MgO + TiO_2)$ ratio of the beschtauite exceeds 0.4 (0.36–0.54, average 0.48). Moreover, a small number of rock samples were distributed in the middle region, and the majority of them were concentrated below the low-pressure curve (Figure 10). This indicates that the petrogenesis of the rocks was associated with the lower crust under high-temperature settings, where mixing of the mantle-derived materials might have occurred.

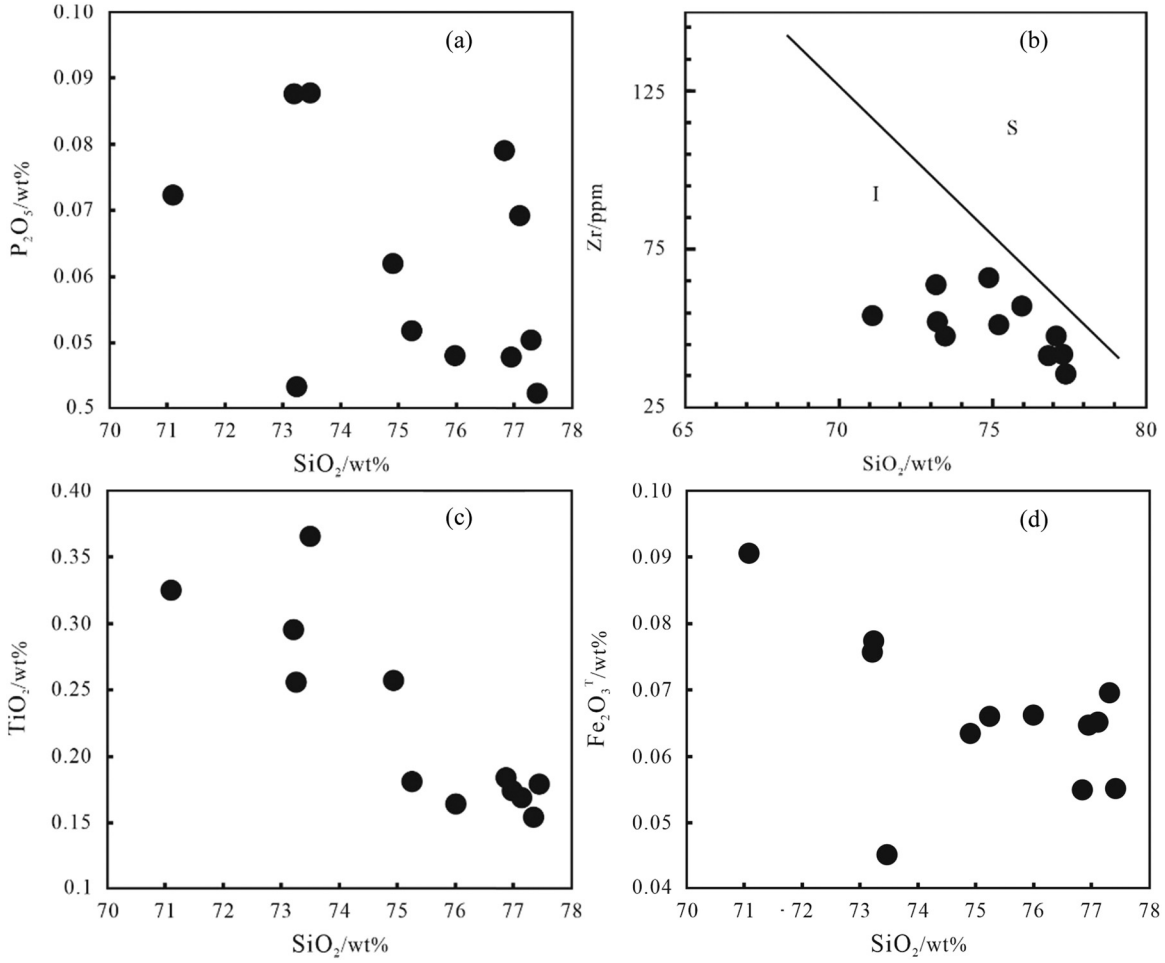

Figure 9: (a) SiO_2–P_2O_5 diagram [109], (b) SiO_2–Zr diagram [120], (c) SiO_2–TiO_2 diagram [109], and (d) SiO_2–$Fe_2O_3^T$ diagram [109].

The beschtauite exhibits strong peraluminous geochemical characteristics (Figure 6d) and a tectonic low-pressure setting (Figure 10). Earlier studies have suggested that strong peraluminous granite demonstrates two tectonic settings as follows: one is high pressure and the other is high temperature [125–131]. The beschtauite in Mengjiaping is concluded to be in a high-temperature tectonic setting, further verifying the petrogenesis via partial crustal melting. Therefore, this beschtauite may have been formed by mantle-derived magma in a high-temperature setting, causing the partial melting of the crustal materials.

7 Structural significance

Geochemical characteristics indicate that Mengjiaping beschtauite is a calc-alkaline–arc tholeiite series, peraluminous granite. The LREEs and HREEs are clearly fractionated, enriching the LREEs and depleting the HREEs. It is enriched in LILEs such as Rb, Th, and K, deficient in HFSEs such as Nb, Ta, and Ti and has the basic characteristics of a typical volcanic-arc granite. Earlier studies have shown that the petrogenesis types of beschtauite are I-type granite [76–80], A-type granite [81–85], and adakite [79,86–89]. Although in this study, the beschtauite La/Yb ratio meets the criteria of adakite (La/Yb > 20) [132–136], the Sr content is considerably lower than the standard for identifying typical adakite (Sr > 400×10^{-6}) [137–139]. So, it is judged that beschtauite may have some similar geochemical characteristics to adakite, but it is not an adakite. In addition, beschtauite is clearly distinguished from A-type granites (Figure 8a–d), and all fall into the I-type granite region in the SiO_2–Zr diagram (Figure 9b). Therefore, Mengjiaping beschtauite is an I-type granite.

Mengjiaping beschtauite demonstrates an arc-related tectonic setting in the isotope study (Figure 11a–d) [140,141]. The results indicate that beschtauite may originate from mantle-derived magma or mixed crust- and mantle-derived magma. In the tectonic-setting identification

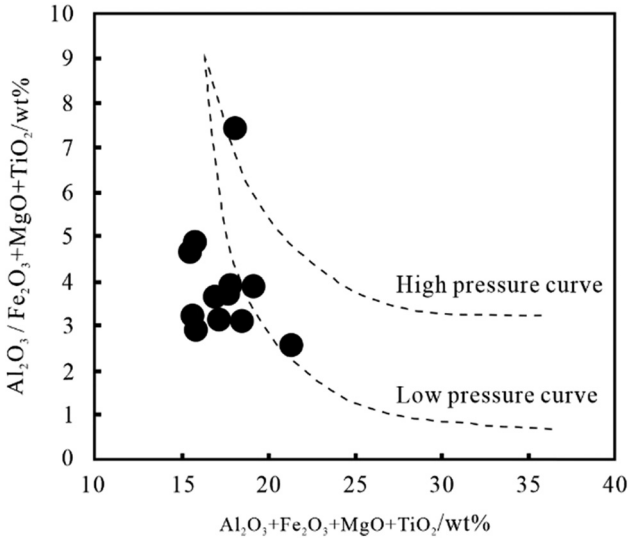

Figure 10: $(Al_2O_3 + Fe_2O_3 + MgO + TiO_2)$–$(Al_2O_3/Fe_2O_3 + MgO + TiO_2)$ diagram [122]. The high-pressure and low-pressure reaction curves are formed by the melting of high-Al olivine basalt and metagreywacke. The interval between the high-pressure and low-pressure curves is the depth range where the crust and mantle are contaminated.

diagram (Figure 12a–d) [142], the rock samples are all cast in the volcanic-arc granite region, indicating that the beschtauite is the product of arc magmatic rocks associated with the subduction of the oceanic crust. The Nb/Ta ratio is 10.06–14.04, which is low (<17). Furthermore, the characteristics of Nb and Ta are deficient relative to LILE. This indicates that the original rock has experienced partial melting under water-bearing conditions, indicating a subduction environment [143]. This conclusion is consistent with the findings of several researchers. Ye et al. suggested that the beschtauite in the Jidong Dalizi iron ore district is a I-type granite, formed in a subduction environment [77]. Lai et al. considered the beschtauite of Songnuo in the Gezan Island arc of Yunnan as an I-type granite, formed in a volcanic-arc tectonic setting and associated with oceanic crustal subduction tectonics [90]. Zhang et al. suggested that the beschtauite in the Duolong mineralized area is a high potassium–calcium–alkaline quasi–aluminous I-type granite with more typical geochemical characteristics of island-arc magmatism and formed in a subduction environment [91]. Sha et al. considered the beschtauite in the Xuejiping copper mining

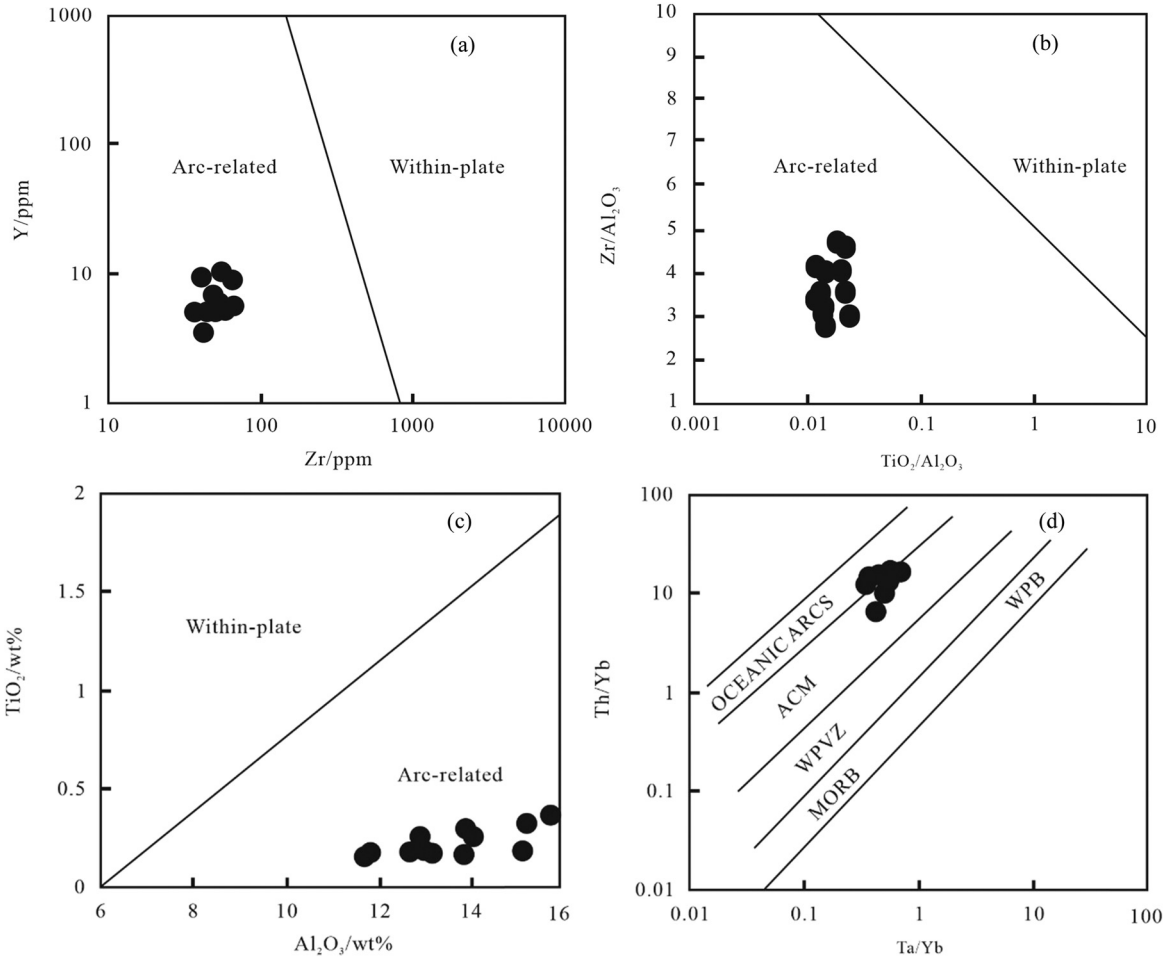

Figure 11: (a) Y–Zr diagram [140], (b) Zr/Al_2O_3–TiO_2/Al_2O_3 diagram [140], (c) TiO_2–Al_2O diagram [140], and (d) Th/Yb–Ta/Yb diagram [141].

area to be an I-type granite, formed in a subduction environment [92]. Liu et al. suggested that the beschtauite of Yunnan Zhuoma is an I-type granite with features of island-arc granite, formed in a subduction environment [93]. In summary, the tectonic setting of beschtauite in this study is a volcanic arc, which is closely related to the subduction of oceanic crust.

Recently, several scholars have determined that the Trans-North China Block is associated with a subduction magmatism event during the Paleoproterozoic [21,53–55]. They proposed that the limited properties of the North China Craton are crucial in the construction of the Trans-North China Block, occurrence of magma activity chronological events, and indication of geochemical characteristics that enable the study of the Trans-North China Block intrusive rocks. Zhao et al. believed that the magmatic activity of 2,200–2,000 Ma in the Trans-North China Block was associated with subduction [53–55]. Wang et al. believed that the main sedimentary setting of the Paleoproterozoic Gantaohe Group in the middle and southern sections of the Taihang Mountains was a set of terrigenous clastic–flysch–carbonate rock-basic volcanic rocks with terrigenous clastic formation, produced in the nearshore setting [144]. The Mengjiaping beschtauite (1,880 ± 69 Ma) studied in this article is associated with a subduction setting. Based on this finding, the Trans-China North Block may be in a subducting tectonic setting. This conclusion is consistent with the earlier results [51,145–147].

The Xuting granite intrusion is nearest to the study area of this article, located ~50 km northeast of the Mengjiaping beschtauite. Not only do they share the same tectonic position but also share similar geochemical characteristics. Both the Xuting granite and beschtauite exhibit high Si (75.95–77.21, 71.1–77.4%, respectively), high Na (2.85–3.54, 3.41–4.78%, respectively), LREE/HREE ratios

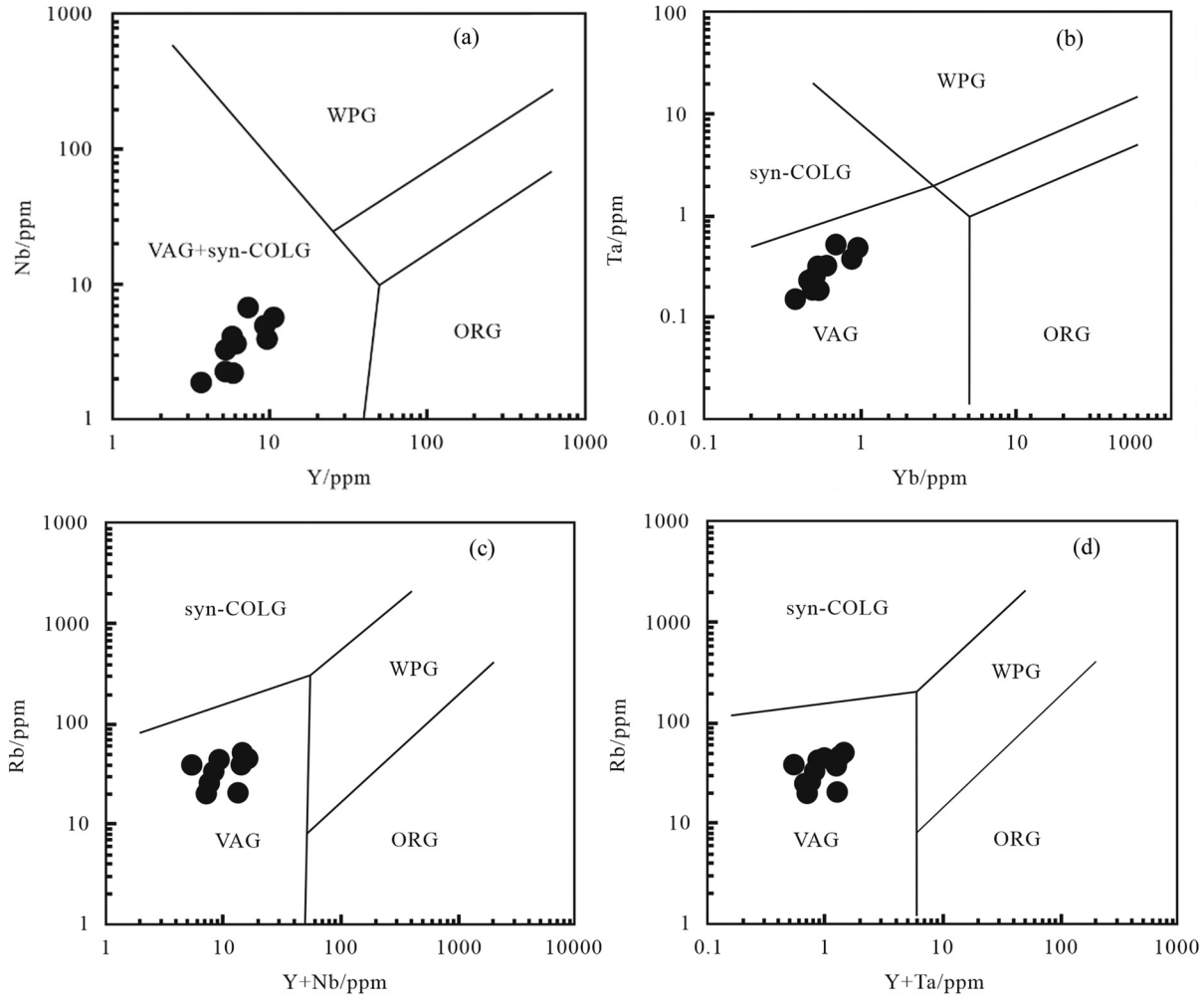

Figure 12: Identification diagram of the tectonic setting [142]: (a) Y–Nb diagram, (b) Yb–Ta diagram, (c) Y + Nb–Rb diagram, and (d) Y + Ta–Rb diagram. ORG – oceanic ridge granite, WPG – intraplate granite, VAG – volcanic-arc granite, and syn-COLG – syncollisional granite.

that are enriched in LREEs and deficient in HREEs (7.29–11.90, 9.66–18.70, respectively). Xuting granite and Mengjiaping beschtauite. Many similar geochemical characteristics indicate that the two may have originated from the same magmatic source area.

Some scholars believe that the central part of the Trans-North China Block was in a tensional rift setting from 2,100 to 1,900 Ma [17,30]. Yang et al. suggested that the bimodal volcanic assemblage of the Xuting granite and the metamorphic basalt of the Gantaohe Group formed in a tensional rift setting. The proportions of basic and acidic rocks vary considerably in bimodal volcanic rocks that were formed in oceanic island-arc settings. The characteristics of basic rocks in this setting are as follows: highly depleted or slightly enriched LREEs, low K, low Ti, low Th, low Nb, enriched LILE, depleted HFSE, and high $\varepsilon Nd(t)$. The characteristics of acidic rocks in this setting are as follows: low K and abundant Nb, depleted LILE, depleted or enriched LREE, obvious negative Eu anomaly, and high $\varepsilon Nd(t)$ [148].

The metamorphic basalt of the Gantaohe Group is a basic rock with the following geochemical characteristics: SiO_2 (48.80×10^{-6} to 53.57×10^{-6}), LREE/HREE (2.2–4.5), Zr/Nb ratio (18.4–22.2), La (6.1×10^{-6} to 8.6×10^{-6}), $\varepsilon Nd(t)$ (4.0, 2.7, −0.8), enriched LILEs (Th and K), and negligibly deficient HSFEs (Nb and Ta) [20]. These characteristics are considerably different from those of the basic rocks in bimodal volcanic rocks formed in a continental rift setting (high LREE/HREE, low Zr/Nb (3–10), low La (50×10^{-6} to 100×10^{-6}), middle $\varepsilon Nd(t)$ (2–5), enriched LILE, and enriched HFSE). The metamorphic basalt is low in K (0.35×10^{-6} to 0.83×10^{-6}), Ti (0.66×10^{-6} to 1.46×10^{-6}), Th (0.4×10^{-6} to 0.7×10^{-6}), and Nb (2.7×10^{-6} to 5.0×10^{-6}). Further, it exhibits flat-type REE distribution patterns, LREE/HREE (3.2–6.4), and enriched LILE (Rb, Sr, and Ba). These geochemical characteristics indicate that this rock developed in an oceanic island-arc setting.

The Xuting granite is an acid rock with the following geochemical characteristics: SiO_2 (75.50×10^{-6} to 77.21×10^{-6}), LREE/HREE (7.3–11.9), $\varepsilon Nd(t)$ (from −14.29 to −0.29), depleted LILE (Sr, Ba, and Ta), and depleted HFSE [17]. These geochemical characteristics are considerably different from those of acidic rocks in bimodal volcanic rocks formed in a continental rift setting (high LREE/HREE, middle $\varepsilon Nd(t)$ (2–5), enriched LILEs, and enriched HFSEs). The Xuting granite is low in K (3.36×10^{-6} to 5.33×10^{-6}), Ti (0.26×10^{-6} to 0.36×10^{-6}), Nb (20.3×10^{-6} to 28.6×10^{-6}), and Th (7.65×10^{-6} to 17.5×10^{-6}). Moreover, it is LILE deficient (Sr, Ba, and Ta), and the Eu-negative anomaly is prominent ($Eu/Eu^* = 0.1–0.35$). These geochemical characteristics indicate that this rock is developed in the oceanic island-arc setting. It is assumed that the bimodal volcanic assemblage composed of metamorphic basalt of the Gantaohe Group and the Xuting granite may also have formed in a subduction tectonic setting.

In summary, we conclude that the Mengjiaping beschtauite was formed in a volcanic-arc tectonic setting. The ocean basin between the Eastern and Western Blocks was not completely closed during 2,090–1,880 Ma and was still in a subduction setting. The formation time of the crystalline basement in the Trans-North China Block should be delayed to 1,880 Ma.

8 Conclusion

The following are the conclusions drawn from the geological fieldwork, petrographic studies, geochemical analysis, and zircon U–Pb chronology research:

The LA-ICP-MS zircon U–Pb age of the beschtauite is 1,880 ± 69 Ma, indicating that the emplacement era is during the Late Paleoproterozoic.

The beschtauite is an I-type granite characterized by high SiO_2, high Na_2O_2, low K_2O, low P_2O_5, and high differentiation as well as peraluminosity, which may have originated from the partial melting of the crust, along with some mantle-derived materials.

The beschtauite formed in a volcanic-arc tectonic setting and is a product of oceanic crustal subduction. The formation age of the crystalline basement of the North China Craton should be after 1,880 Ma.

Abbreviations

HFSE	high-field strength elements
HREE	heavy rare-earth elements
LILE	large ionic lithophile elements
LREE	light rare-earth elements
REE	rare-earth elements
CL	cathodoluminescence
LA-ICP-MS	laser ablation inductively coupled plasma mass spectrometry
MSWD	mean square weighted deviation
N	number of calculated measure points
2σ	confidence degree error

Acknowledgements: We sincerely appreciate the editors and reviewers for their constructive comments. We also

thank Cai Kui, Zhang Minjie, and Yu Yanqiu who critically read the early draft and helped with geochemical analyses.

Funding information: Doctoral Research Startup Fund of Hebei GEO University (BQ2018031).

Author contributions: Conceptualization – Tian, H.F., Chen, W.J., Zou, P.J., and Jin, M.Q.; methodology – Tian, H.F., Cui, X.T., Chen, H.T., and Wang, S.; visualization – Tian, H.F., Hu, X.F., Han, S.N., and Liang, X.; writing – original draft preparation, Tian, H.F., Zou, C.J., and Zhao, L.; and writing – review and editing, Tian, H.F., Li, G.Y., Choi, J.Y., and Luan, W.L. All authors have read and agreed to the published version of the manuscript.

Conflict of interest: Authors state no conflict of interest.

References

[1] Zhang RY, Sun Y. Formation and evolution of Early Precambrian basement in the southern North China Craton. Acta Petrol Sin. 2017;33(10):3027–41 (in Chinese with English abstract).

[2] Xiao LL, Liu FL. Precambrian metamorphic history of the metamorphic complexes in the Trans–North China Orogen. North China Craton Acta Petrol Sin. 2015;31(10):3012–44 (in Chinese with English abstract).

[3] Shen QH, Geng YS, Song HZ. Constituents and evolution of the metamorphic basement of the North China Craton. Acta Geosci Sin. 2016;37(4):387–406 (in Chinese with English abstract).

[4] Zhao GC, Wilde SA, Cawood PA, Lu LZ. Thermal evolution of the Archaean basement rocks from the eastern part of the North China Craton and its bearing on tectonic setting. Int Geol Rev. 1998;40(8):706–21.

[5] Zhao GC, Wilde SA, Cawood PA, Sun M. Archean blocks and their boundaries in the North China Craton: lithological, geochemical, structural and P–T path constraints and tectonic evolution. Precambrian Res. 2001;107(1):45–73.

[6] Zhao GC, Sun M, Wilde SA, Sanzhong L. Late Archean to Paleoproterozoic evolution of the North China Craton: Key issues revisited. Precambrian Res. 2005;136(2):149–72.

[7] Zhai MG, Bian AG, Zhao TP. The amalgamation of the supercontinent of North China craton at the end of Neoarchean and its breakup during the Late Paleoproterozoic and Meso–Proterozoic. Sci China Ser D: Earth Sci. 2000;43(1):219–32.

[8] Zhai MG. Lower crust and lithospheric mantle beneath the North China Craton before the Mesozoic lithospheric disruption. Acta Petrol Sin. 2008;24(10):2185–204 (in Chinese with English abstract).

[9] Kusky TM, Li JH. Paleoproterozoic tectonic evolution of the North China Craton. J Asian Earth Sci. 2003;22:383–97.

[10] Faure M, Trap P, Lin W, Monié P, Bruguier O. The formation of the North China Crat on by two Paleoproterozoic continental collisions in Lüliang–Hengshan–Wutaishan–Fuping massifs massifs. Episodes. 2007;30:1–12.

[11] Trap P, Faure M, Lin W, Monié P. Late Paleoproterozoic (1900–1800 Ma) nappe stacking and polyphase deformation in the Hengshan–Wutaishan area: Implications for the understanding of the Trans–North–China Belt, North China Craton. Precambrian Res. 2007;156(1–2):85–106.

[12] Trap P, Faure M, Lin W, Bruguier O, Monié P. Contrasted tectonic styles for the Paleoproterozoic evolution of the North China Craton. Evidence for a ~2.1 Ga thermal and tectonic event in the Fuping Massif. J Struct Geol. 2008;30:1109–25.

[13] Trap P, Faure M, Lin W, Monié P, Meffre S, Melleton J. The Zanhuang Massif, the second and eastern suture zone of the Paleoproterozoic Trans–North China Orogen. Precambrian Res. 2009;72(1–2):80–98.

[14] Trap P, Faure M, Lin W, Meffre S. The Luliang Massif: a key area for the understanding of the Paleoproterozoic Trans–North China Belt. North China Craton. Geolog Soc London Special Pub. 2009;323(1):99–125.

[15] Trap P, Faure M, Lin W, Augier R, Fouassier A. Syn–collisional channel flow and exhumation of Paleoproterozoic high pressure rocks in the Trans–North China Orogen: The critical role of partial–melting and orogenic Bending. Gondwana Res. 2011;20(2–3):498–515.

[16] Trap P, Faure M, Lin W, Le Breton N, Monié P. Paleoproterozoic tectonic evolution of the Trans–North China Orogen: toward a comprehensive model. Precambrian Res. 2012;222:191–211.

[17] Yang CH, Du LL, Ren LD, Song HX, Wan YS, Xie HQ, et al. Petrogenesis and geodynamic setting of Jiandeng potassic granite at the end of the Neoarchean in Zanhuang Complex, North China Craton. Earth Sci Front. 2011;18(2):62–78 (in Chinese with English abstract).

[18] Xiao C, Li M, Yang W, Hu M, Li C. The age and petrogenesis of the Xuting granite in the Zanhuang Complex, Hebei Province: Constraints on the structural evolution of the Trans–North China Orogen, North China Craton. Acta Petrol Sin. 2011;27(4):1003–16 (in Chinese with English abstract).

[19] Yang CH, Du LL, Ren LD, Song HX, Wan YS. Stratigraphic division and correlation of the early precambrian of the North China craton and magma evolution. Science Press; 2015. p. 1–10.

[20] Xie H, Liu D, Yin X, Zhou H, Yang C, Du L, et al. Formation age and tectonic environment of the Gantaohe Group, North China craton: geology, geochemistry, SHRIMP zircon geochronology and Hf–Nd isotopic systematics. Chin Sci Bull. 2012;57:4735–45 (in Chinese with English abstract).

[21] Zhao GC, Cawood PA. Precambrian Geology of China. Precambrian Res. 2012;222:13–54.

[22] Kusky TM. Geophysical and geological tests of tectonic models of the North China Craton. Gondwana Res. 2011;20:26–35.

[23] Kusky TM. Comparison of results of recent seismic profiles with tectonic models of the North China Craton. J Earth Sci. 2011;22:250–59.

[24] Deng H, Kusky TM, Polat A, Wang L, Wang JP, Wang SJ. Geochemistry of Neoarchean mafic volcanic rocks and late mafic dikes in the Zanhuang Complex, Central Orogenic Belt,

North China Craton: implications for geodynamic setting. Lithos. 2013;175:193–212.
[25] Deng H, Kusky T, Polat A, Wang J, Wang L, Fu J, et al. Geochronology, mantle source composition and geodynamic constraints on the origin of Neoarchean mafic dikes in the Zanhuang Complex, Central Orogenic Belt, North China Craton. Lithos. 2014;205:59–378.
[26] Wang JP, Kusky TM, Polat A, Wang L, Deng H, Wang SJ. A late Archean tectonic mélange in the Central Orogenic Belt. North China Craton Tectonophys. 2013;608:929–46.
[27] Wang JP, Kusky TM, Wang L, Polat A, Deng HA. Neoarchean subduction polarity reversal event in the North China Craton. Lithos. 2015;220:133–46.
[28] Wang J, Kusky T, Wang L, Polat A, Wang S, Deng H, et al. Petrogenesis and geochemistry of circa 2500 Ma granitoids in the zanhuang massif: implications for magmatic source and neoarchean metamorphism of the north china craton. Lithos. 2017;268:149–62.
[29] Wang J, Kusky T, Wang L, Polat A, Deng H, Wang C, et al. Structural relationships along a Neoarchean arc–continent collision zone, North China craton. Geol Soc Am Bull. 2017;129:59–75.
[30] Du L, Yang C, Wyman DA, Nutman AP, Lu Z, Song H, et al. 2090–2070 Ma A–type granitoids in Zanhuang Complex: Further evidence on a Paleoproterozoic rift–related tectonic regime in the Trans–North China Orogen. Lithos. 2016;254–255:18–35.
[31] Kusky TM, Polat A, Windley BF, Burke KC, Dewey JF, Kidd WSF, et al. Insights into the tectonic evolution of the North China Craton through comparative tectonic analysis: A record of outward growth of Precambrian continents. Earth Sci Rev. 2016;162:387–432.
[32] Tang L, Santosh M, Tsunogae T, Maruoka T. Paleoproterozoic meta–carbonates from the central segment of the Trans–North China Orogen: Zircon U–Pb geochronology, geochemistry, and carbon and oxygen isotopes. Precambrian Res. 2016;284:14–29.
[33] Tang L, Santosh M, Tsunogae T, Maruoka T. Reply to comment by Wang et al. on "Paleoproterozoic meta–carbonates from the central segment of the Trans–North China Orogen: Zircon U–Pb geochronology, geochemistry, and carbon and oxygen isotopes". Precambrian Res. 2017;294:350–3.
[34] Li SS, Santosh M, Teng XM, He XF. Paleoproterozoic arc–continent collision in the North China Craton: evidence from the Zanhuang Complex. Precambrian Res. 2016;286:281–305.
[35] Li SS, Santosh M, Teng XM, He XF. Reply to comment by Wang et al. on "Paleoproterozoic arc continent collision in the North China Craton: Evidence from the Zanhuang Complex". Precambrian Res. 2018;304:174–7.
[36] Shi JP. Geochronology and geochemistry of the Paleoproterozoic A–type granites in the southern margin of the Central North China Craton. Jilin Univ China. 2017;33(10):3042–56 (in Chinese with English abstract).
[37] Li L, Yang YQ, Yang CH, Du LL, Song HX, Ren LD, et al. The petrogenesis and tectonic setting of ca. 2500 Ma A–type granite in the Zanhuang complex: An example from the Huangcha granite. Acta Petrolgica Sin. 2017;33(9):2850–66 (in Chinese with English abstract).
[38] Zang F. The neoarchean–paleoproterozoic geological evolution of the zanhuang complex in central segment of the north china craton. PhD thesis, Chin Acad Geol Sci, China; 2019.
[39] Xiao LL, Liu FL, Zhang J. Records and its geological implication of metamorphic ages of ca. 2500 Ma and ca. 1900 Ma from the Zuoquan metamorphic complex in the Trans–North China Orogen. Acta Petrol Sin. 2019;35(4):969–88 (in Chinese with English abstract).
[40] Zhao Q. Zircon U–Pb geochronology, geochemistry and its geological implication for the Neoarchean Rocks of Zhongtiaoshan Area in Southern North China Craton. PhD thesis, Shanxi Norm Univ, China; 2019.
[41] Zhang SH, Zhang R, Zhou J. LA–ICP–MS Zircon U–Pb age, geochemical characteristics of the Paleoproterozoic metamorphosed mafic dykes in Zhongtiao Mountains, Shanxi Province, and their geological implications. Geol Rev. 2019;92:2535–42 (in Chinese with English abstract).
[42] Feng JP, Ouyang ZJ, Ma HY, Fan MM, Ma J. U–Pb chronology, geochemical characteristics and significance of the Taojiayao basic dike swarms in the Zhongtiao Mountain, southeastern margin of North China Craton. Acta Geol Sin. 2020;94(2):573–86 (in Chinese with English abstract).
[43] Du LL, Yang CH, Song HX, Wang JL, Duan QS, Huang ZQ. Neoarchean–Paleoproterozoic multi-period geological events and structural properties of the Fuping complex in the North China Craton. Earth Sci. 2020;45(9):3179–95 (in Chinese with English abstract).
[44] Liu PH, Tian ZH, Wen F, Zhou WP, Wang YL. Multiple high–grade metamorphic events of the Jiaobei terrane, North China craton: new evidences from Zircon U–Pb ages and trace elements compositions of garnet amphilbote and granitic leucosomes. Earth Sci. 2020;45(9):3196–216 (in Chinese with English abstract).
[45] Diwu CR. Growth and evolution of the Archean continental crust in the southern part of the North China Craton. Acta Petrol Sin. 2021;37(2):317–40.
[46] Shi KX, Wang CM, Du B, Chen Q, Zhu JX, Rao SC, et al. Ca. 1900–1800 Ma continent–continent collision in the south–eastern North China Craton: Evidence from granite–greenstone belt in the Jiaobei Terrane. Earth Sci Front. 2021:1–24. doi: 10.13745/j.esf.sf.2021.1.59 (in Chinese with English abstract).
[47] Liu JH, Qian XL, Huang XN, Liu SW. Tectonic framework of North China Block and its cratonization in the early Precambrian. Acta Petrol Sin. 2000;16(1):1–10 (in Chinese with English abstract).
[48] Guo JH, O'Brien PJ, Zhai MG. High–pressure granulites in the Sanggan area, North China Craton: Metamorphic evolution, P–T paths and geotectonic significance. J Metamorphic Geol. 2002;20:741–56.
[49] Guo JH, Sun M, Chen FK, Zhai MG. Sm–Nd and SHRIM P U–Pb zircon geochronology of high pressure granulites in the Sanggan area, North China Craton: Timing of Paleoproterozoic continent al collision. J Asian Earth Sci. 2005;24:629–42.
[50] Liu SW, Li HJ, Pan YM, Zhang J, Li QG, Huang XN. The chronology and geochemical constraints of the archaean lands from taihang mountain to heng mountain. Adv Nat Sci. 2002;12(8):826–33 (in Chinese with English abstract).

[51] Liu SW, Li QG, Zhang LE. Geology, geochemistry of metamorphic volcanic rock suite in Precambrian Yejishan Group, Luliang mountains and its tectonic implications. Acta Petrol Sin. 2009;25(3):547–60 (in Chinese with English abstract).
[52] Zhao GC, Wilde SA, Cawood PA, Sun M. SHRIMP U–Pb zircon ages of the Fuping Complex: Implications for Late Archean to Paleoproterozoic accretion and assembly of the North China Crat on. Am J Sci. 2002;302(3):191–226.
[53] Zhao GC, Sun M, Wilde SA, Sanzhong L, Liu S, Zhang J. Composite nature of the North China granulite–facies belt: Tectonothermal and geochronological constraints. Gondwana Res. 2006;9:337–48.
[54] Zhao GC, Wilde SA, Sun M, Li S, Li X, Zhang J. SHRIMP U–Pb zircon ages of granitoid rocks in the Lǜliang Complex: Implications f or the accretion and evolution of the Trans–North China Orogen. Precambrian Res. 2008;160:213–26.
[55] Zhao GC, Wilde SA, Guo J, Cawood PA, Sun M, Li X. Single zircon grains record two Paleoproterozoic collisional events in the North China Crat on. Precambrian Res. 2010;177(3–4):266–76.
[56] Zhao GC, Yin C, Guo J, Sun M, Li S, Li X. Metamorphism of the Lüliang amphibolite: implications for the tectonic evolution of the North China Craton. Am J Sci. 2010;310(10):1480–502.
[57] Kröner A, Wilde SA, O'Brien PJ, Li JH, Passchier CW, Walte NP. Field relationships, geochemistry, zircon ages and evolution of a late Archean to Paleoproterozoic lower crustal section in the Hengshan Terrain of Northern China. Acta Geol Sin. 2005;79:605–29.
[58] Kröner A, Wilde SA, Zhao GC, O'Brien PJ, Sun M, Liu DY. Zircon geochronology of mafic dykes in the Hengshan Complex of northern China: Evidence for Late Paleoproterozoic rifting and subsequent high–pressure event in the North China Craton. Precambrian Res. 2006;146:45–67.
[59] Faure M, Trap P, Lin W, Monié P, Bruguier O. Polyorogenic evolution of the Paleoproterozoic Trans–North China Belt–New insights from the Lǜliangshan–Hengshan–Wutaishan and Fuping massifs. Episodes. 2007;30(2):96–107.
[60] Wan YS, Liu DY, Wang W, Song T, Kröner A, Dong C. Provenance of Meso–to Neoproterozoic cover sediments at the Ming Tombs, Beijing, North China Craton: An integrated study of U–Pb dating and Hf isotopic measurement of detrital zircons and w hole–rock geochemistry. Gondwana Res. 2011;20(1):219–42.
[61] Yin C, Zhao G, Guo J, Sun M, Xia X, Zhou X, et al. U–Pb and Hf isotopic study of zircons of the Helanshan Complex: Constrains on the evolution of the Khondalite Belt in the West ern Block of the North China Craton. Lithos. 2011;122:25–38.
[62] Wang X, Huang X, Ma J, Zhong J, Yang Q. Hf–Nd isotopes of the early precambrian metamorphic complexes in the southern segment of the trans–north china orogen: implications for crustal evolution. Geotectonica Et Metallogenia. 2015;39(6):1108–18 (in Chinese with English abstract).
[63] Chen Y, Zhang J, Liu J, Yin CQ, Wang LJ, Li X. Differences in the genesis of Late Archean TTG rocks between the central orogenic belt of the North China Craton and the eastern landmass and their geological significance. China Peace Audiov Electron Publ House. 2018;23:1–7 (in Chinese with English abstract).
[64] Yang CH, Du LL, Song HX, Duan QS, Wang JL, Huang ZQ, et al. Geochronology and petrogenesis of neoarchean yanzhuang syenogranites from sushui complex in the zhongtiao mountains: implications for the crustal evolution of the north china craton. Earth Sci. 2020;45(9):3161–78 (in Chinese with English abstract).
[65] Li TG, Wu G, Chen GZ, Wu H, Wang GR, Yang F. Genesis of linghu gold deposit in xiaoqinling ore district, the southern margin of north china craton, china: evidence from fluid inclusions, h–o and s–pb isotopic compositions. J Earth Sci Environ. 2020;42(5):569–83 (in Chinese with English abstract).
[66] Duan QS, Song HX, Du LL, Ren LD, Geng YS, Wang JL, et al. The magmatic activity in paleoproterozoic global magmatic quiescence: take the ~2300 ma henglingguan granites from zhongtiao mountains in the southernnorth china craton as an example. Earth Sci. 2020;45(9):3372–85 (in Chinese with English abstract).
[67] Huang B. Neoarchean accretionary–to–collisional orogenesis in the southern North China Craton and its geodynamic implications. PhD thesis, China Univ Geosci, China; 2020.
[68] Shi Q. Metamorphic anatexis and tectonic significance of early Precambrian garnet granite in the northern margin of North China Craton. PhD thesis, Jilin Univ China, China; 2020.
[69] Xiao LL, Jiang ZS.Geochemistry and Tectonic Environment of Amphibolites of the Zanhuang Metamorphic Complex. Bull Mineralogy Petrology Geochem. 2010;29(4):339–47 (in Chinese with English abstract).
[70] Xiao LL, Wang GD. Zircon U–Pb dating of metabasic rocks in the Zanhuang metamorphic complex and its geological significance. Acta Petrol Et Mineralogica. 2011;30(5):781–94 (in Chinese with English abstract).
[71] Xiao LL, Lu JS, Wang GD, Cai J, Wu CM. Geochemistry metamorphic evolution and its tectonic implications of amphibolites in the southwest area of the Zanhuang complex. Acta Petrol Sin. 2012;28(9):2807–18 (in Chinese with English abstract).
[72] Xiao LL, Liu FL, Liu JH, Liu PH, Shi JR, Cai J. Geochemistry and its tectonic implications of the Zuoquan–Zanhuang complex. Acta Petrol Sin. 2013;29(2):533–50 (in Chinese with English abstract).
[73] Liu CH, Zhao GC, Sun M, Zhang J, Yin C. U–Pb geochronology and Hf isotope geochemistry of detrital zircons from the Zhongtiao Complex: constraints on the tectonic evolution of the Trans–North China Orogen. Precambrian Res. 2012;222:159–72.
[74] Shi KX, Wang CM, Du B, Chen Q, Zhu JX. Neoarchean to Paleoproterozoic tectonic evolution of the Trans–North China Orogen, North China Craton: Evidence from zircon U–Pb geochronology, Lu–Hf isotopes, and geochemistry of the Zanhuang Complex. Geol J. 2020;56(3):1236–57.
[75] Zou L, Guo JH, Yang CH, Du LL, Liu PH. The P–T–t path of pelitic gneisses in the Zanhuang Complex: Further constraints on the Paleoproterozoic tectonic evolution of the Trans–North China Orogen, North China Craton. J Asian Earth Sci. 2021;210:104701.

[76] Hu SQ, Zhou GF, Peng SB, Zhang XJ, Yi SH, Tang GS. Chronology and geochemical characteristics of quartz monzonite (porphyry) in the Dali copper-molybdenum deposit and Its geological significance. Acta Geosc Sin. 2012;33(1):23–37 (in Chinese with English abstract).
[77] Ye LN, Sun FY, Wang L, Liu JL, Zhang YT. Zircon U–Pb geochronology and Hf isotopic composition of the quartz monzonite porphyry intrusion from east Jilin Province. Earth Sci. 2020;45(5):1544–55 (in Chinese with English abstract).
[78] Tang YW, Xie YL, Li YX, Qiu LM, Liu BS, Li Y, et al. Geochemical characteristics and zircon LA–ICP–MS U–Pb ages of quartz–monzonite porphyry in Anji polymetallic ore district of Zhejiang and their geological Implications. Geoscience. 2012;26(4):647–55 (in Chinese with English abstract).
[79] Ye F, Dong GC, Ren JX, Gong LY, Li MX, Wang Q, et al. Zircon U–Pb geochronology, geochemical characteristics and geological significance of Huangyugou intrusion, Shanxi province. Geoscience. 2021;35(3):787–97 (in Chinese with English abstract).
[80] Wang J, Hu H, Ye ZH, Li K, Cheng ZW. Rock geochemistry, genesis and metallogenic potential analysis in Chuankeng, Shangrao, Jiangxi. Energy Res Manag. 2020;1:55–62 (in Chinese with English abstract).
[81] Li HY, Wang YP, Wu WB, Li C, Liu YJ, Wang XL. Zircon U–Pb dating , geochemical characteristics and geological significance of beschtauite in Yuanjiapu, eastern Liaoning. J Guilin Univ Technol. 2019;39(3):551–7 (in Chinese with English abstract).
[82] Li NB, Luo Y, Guo SL, Jiang YH, Zeng LJ, Niu HC. Zircon U–Pb geochronology and Hf isotope geochemistry of metamorphic quartz–monzonite porphyry from Tongkuangyu area, Zhongtiao Mountain and its geological implications. Acta Petrol Sin. 2013;29(7):2416–24 (in Chinese with English abstract).
[83] Yu ZQ, Chen WF, Chen PR, Wang KX, Fang QC, Tang XS, et al. Chemical composition and Sr isotopes of apatite in the Xiangshan A–type volcanic-intrusive complex, Southeast China: new insight into petrogenesis. J Asian Earth Sci. 2018;172:66–82.
[84] Guan YC, Yang ZF, Zhu XY, Zou T, Cheng XY, Tang L, et al. Petrogenesis and geological significance of the Beidashan complex rock mass, inner Mongolia. Miner Exploration. 2017;8(6):1054–68 (in Chinese with English abstract).
[85] Shen L, Zhao SJ, Yu HY, Liu ZH, Zhou YS, Su JG, et al. Geochemical characteristics and zircon U–Pb ages of porphyroclastic lava in the Bayaerhushuo area, the south- central segment of Great Xing'an Range, and its geological significance. Geol Bull China. 2019;38(8):1314–26 (in Chinese with English abstract).
[86] Wang H, Zhang JR, Zhou Q, Sun ZM, Wang YW, Chen G. Zircon U–Pb age and geochemistry of the Guangmashan monzonitic porphyry in Ninglang, Yunnan Province. Geol Bull China. 2019;38(11):1858–66 (in Chinese with English abstract).
[87] Li M, Guo Y, Li Z, Wang H, Zhang J. Petrogenesis analysis of the oligocene porphyry in Xifanping of Yanyuan. Sichuan Acta Geol Sin. 2019;93(3):622–32 (in Chinese with English abstract).
[88] Gao ZX, Xie CM, Ren YS, Liu JH, Li LH, Hao YJ. LA–ICP–MS zircon U–Pb ages and geochemical characteristics of the Azarang rock mass in the Songdo area, southern Tibet. Earth Sci. 2019;44(7):2353–67 (in Chinese with English abstract).
[89] Zeng PS, Li WC, Wang HP, Li H. The Indosinian Pulang superlarge porphyry copper deposit in Yunnan, China: Petrology and chronology. Acta Petrol Sin. 2006;22(4):989–1000 (in Chinese with English abstract).
[90] Lai AQ, Li WC, Liu XL, Yang FC, Li Z. Zircon U–Pb Dating, geochemical characteristics of Songnuo quartz monzonite porphyries in the Gezan Arc, Yunnan Province, and their geological significance. Geol Rev. 2016;62(4):955–69 (in Chinese with English abstract).
[91] Zhang H, Liu H, Liu SS, Ma DF, Zhang H, Huang HX, et al. Petrogenesis of the early cretaceous Jiuqianxi I-type granite pluton, Bangonghu–Nujiang metallogenic belt, northern Tibet. China Min Mag. 2017;26(11):162–78.
[92] Sha JZ, Luo CD, Wang P. Tectonic environment and metallogenic significance of magmatite in Xuejiping copper mine, northwest Yunnan. Mineral Resources and Geology. 2016;30(5):703–11 (in Chinese with English abstract.
[93] Liu XL, Li WC, Zhang N. Zircon U–Pb age and geochemical characteristics of the quartz monzonite porphyry from the Zhuoma deposit, Yunnan, China. Bull Mineral Petrol Geochem. 2016;35(1):109–17 (in Chinese with English abstract).
[94] Liu GX, Zhang CP, Lyu JC, Zhang P. Zircon U–Pb chronology of quartz monzoporphyry in Jiawula Pb–Zn–Ag deposit. Daxinganling Mt Geol Resour. 2018;27(5):424–30 (in Chinese with English abstract).
[95] Zhou J, Wang GH, Cui YL. Petrogenesis and tectonic indication of the Eocene porphyry in the Fenshuiling mining area, western Yunnan Province: Constraints from bulk geochemistry, zircon U–Pb geochronology and Hf isotopes. Geol Exploration. 2017;53(6):1070–89.
[96] Cui D, Chen YL, Li DP, Wang SH, Chen X. Zircons U–Pb dating and hf isotopic composition of clastic sedimentary rock in the nansi formation, gantaohe group, north china craton and its tectonic significance. Geol Rev. 2015;61(2):425–42 (in Chinese with English abstract).
[97] Peng P, Yang SY, Su XD, Wang X, Zhang J, Wang C. Petrogenesis of the 2090 Ma zanhuang ring and sill complexes in north china: a bimodal magmatism related to intracontinental process. Precambrian Res. 2017;303:153–70.
[98] Liu CH, Zhao GC, Liu FL, Sun M, Zhang J, Yin CQ. Zircons U–Pb and Lu–Hf isotopic and whole–rock geochemical constraints on the Gantaohe Group in the Zanhuang Complex: Implications for the tectonic evolution of the Trans–North China orogen. Lithos. 2012;146–47:80–92.
[99] Ju ZY, Zhang YH, Li Q, Gao DJ, Li SZ. Regional geology of Tianjin, Beijing. Hebei Province: Geological Publishing House; 1989.
[100] Yuan HL, Gao S, Liu XM, Li H, Günther D, Wu F. Accurate U–Pb age and trace element determinations of zircon by laser ablation–inductively coupled plasma–mass spectrometry. GeostGeoanalytical Res. 2004;28(3):353–70.
[101] Andersen T. Correction of common lead in U–Pb analyses that do not report ^{204}Pb. Chem Geo. 2002;192(1–2):59–79.
[102] Liu Y, Hu Z, Zong K, Gao C, Gao S, Xu J, et al. Reappraisement and refinement of zircon U–Pb isotope and trace element analyses by LA–ICP–MS. Chin Sci Bull. 2010;55:1535–46.

[103] Hoskin PWO, Schaltegger U. The composition of zircon and igneous and metamorphic petrogenesis. Rev Mineralogy Geochem. 2003;53(1):27–62.
[104] Allègre CJ, Minster JF. Quantitative models of trace element behavior in magmatic processes. Earth Planet Sci Lett. 1978;38(1):1–25.
[105] Taylor SR, Mclennan SM. The continental crust: Its composition and evolution. United States; 1985. p. 312.
[106] Maniar PD, Piccoli PM. Tectonic discrimination of granitoids. Geol Soc Am Bull. 1989;101(5):635–43.
[107] Sun SS, McDonough WF. Chemical and isotopic systematics of oceanic basalts: Implications for mantle composition and process. Geol Soc Spec Publ. 1989;42:313–26.
[108] Champion DC, Chappell BW. Petrogenesis of felsic I-type granites: An example from northern Queensland. Trans R Soc Edinb Earth Sci. 1992;83:115–26.
[109] Chappell BW, White AJR. I- and S-type granites in the Lachlan Fold Belt. Trans R Soc Edinburgh: Earth Sci. 1992;83:1–26.
[110] Hine R, Williams IS, Chappell BW, White AJR. Contrasts between I- and S-type granitoids of the Kosciusko Batholith. J Geol Soc Aust. 1978;25(3–4):219–34.
[111] King PL, Chappell BW, Allen CM, White AJR. Are A-type granites the high-temperature felsic granites? Evidence from fractionated granites of the Wangrah Suite. Australian J Earth Sci. 2001;48(4):501–14.
[112] Chappell BW. Aluminium saturation in I– and S–type granites and the characterization of fractionated haplogranites. Lithos. 1999;46:535–51.
[113] Watson EB. Zircon saturation in felsic liquids: Experimental results and applications to trace element geochemistry. Contrib to Mineral Petrol. 1979;70(4):407–19.
[114] Watson EB, Harrison TM. Zircon saturation revisited: Temperature and composition effects in a variety of crustal magma types. Earth Planet Sci Lett. 1983;64(2):295–304.
[115] Wu FY, Li XH, Yang JH, Zheng YF. Discussions on the petrogenesis of granite. Acta Petrol Sin. 2007;23(6):1217–38.
[116] Pichavant M, Montel JM, Richard LR. Apatite solubility in peraluminous liquids: Experimental data and an extension of the Harrison-Watson model. Geochimica et Cosmochimica Acta. 1992;56(10):3855–61.
[117] Zen EA. Aluminum enrichment in silicate melts by fractional crystallization: Some mineralogic and petrographic constraints. J Petrology. 1986;27(5):1095–117.
[118] Gao LE, Zeng LS, Asimow PD. Contrasting geochemical signatures of fluid-absent versus fluid-fluxed melting of muscovite in metasedimentary sources: the Himalayan leucogranites. Geology. 2017;45(1):39–42.
[119] Wu FY, Liu ZC, Liu XC, Ji WQ. Himalayan leucogranite: petrogenesis and implications to orogenesis and plateau uplift. Acta Petrol Sin. 2015;31(1):1–36.
[120] Collins WJ, Beams SD, White AJR, Chappell BW. Nature and origin of A–type granites with particular reference to southeastern Australia. Contrib Miner Pet. 1982;80(2):189–200.
[121] Whalen JB, Currie KL, Chappell BW. A–type granites: geochemical characteristics, discrimination and petrogenesis. Contributions Mineralogy & Petrology. 1987;95(4):407–19.
[122] Douce AEP. What do experiments tell us about the relative contributions of crust and mantle to the origin of granitic magmas. Geolog Soc London Special Publ. 1999;168(1):55–75.
[123] Chen B, Arakawa Y. Elemental and Nd–Sr isotopic geochemistry of granitoids from the west junggar fold–belt NW (China), with implications for phanerozoic continental growth. Geochimica Et Cosmochimica Acta. 2005;69(5):1307–20.
[124] Qiu JS, Xiao E, Hu J, Xu XS, Jiang SY, Li Z. Petrogenesis of highly fractionated I–type granites in the coastal area of northeastern Fujian Province: constraints from zircon U–Pb geochronology, geochemistry and Nd–Hf isotopes. Acta Petrol Sin. 2008;24(11):2468–84 (in Chinese with English abstract).
[125] Richards JP. Magmatic to hydrothermal metal fluxes in convergent and collided margins. Ore Geol Rev. 2011;40(1):1–26.
[126] Wang XS, Bi XW, Leng CB, Zhong H, Tang HF, Chen YW, et al. Geochronology and geochemistry of Late Cretaceous igneous intrusions and Mo–Cu–(W) mineralization in the southern Yidun Arc, SW China: implications for metallogenesis and geodynamic setting. Ore Geol Rev. 2014;61:73–95.
[127] Wu F, Jahn B, Wilde SA, Lo CH, Yui TF, Lin Q, et al. Highly fractionated I–type granites in NE China (II): Isotopic geochemistry and implications for crustal growth in the Phanerozoic. Lithos. 2003;67(3–4):191–204.
[128] Valley JW, Lackey JS, Cavosie AJ. Billion years of crustal maturation: oxygen isotope ratios of magmatic zircon. Contrib to Mineral Petrol. 2005;150(6):561–80.
[129] Wedepohl KH. The composition of the continental crust. Geochim Et Cosmochim Acta. 1995;59:1217–32.
[130] Strong DF, Hanmer SK. The leucogranites of southern Brittany: origin by faulting, frictional heating, fluid flux and fractional melting. Can Mineral. 1981;19:163–76 (in Chinese with English abstract).
[131] Pitcher WS. Granite type and tectonic environment. In: Hus KJ, editor. Mountain Building Processes. London: Academic Press; 1982. p. 19–40
[132] Pearce JA. Trace element characteristics of lavas from destructive plate boundaries. In: Thorpe RS, editor. Orogenic Andesites and Related Rocks. Chichester, England: John Wiley and Sons; 1982. p. 525–48
[133] Harris NBW, Pearce JA, Tindle AG. Geochemical characteristics of collision–zone magmatism. London: Geolo Soc London, Special Publ. 1986;19(1):67–81.
[134] Wickham SM. Crustal anatexis and granite petrogenesis during low–pressure regional metamorphism: the trois seigneurs massif, Pyrenees, France. J Petrology. 1987;28(1):127–69.
[135] Finger F, Roberts MP, Haunschmid B, Schermaier A, Steyrer HP. Variscan granitoids of central Europe: their typology, potential sources and tectonothermal relations. Mineralogy Petrology. 1997;61(1–4):67–96.
[136] Sylvester PJ. Post–collisional strongly peraluminous granites. Lithos. 1998;45(1–4):29–44.
[137] Defant MJ, Drummond MS. Derivation of some modern arc-magmas by melting of young subducted lithosphere. Nature. 1990;347(6294):662–65.
[138] Defant MJ, Drummond MS. Mount St. Helens: potential example of the partial elting of the subducted lithosphere in a volcanic arc. Geology. 1993;21(6):547–50.
[139] Drummond MS, Defant MJ, Kepezhinskas PK. Petrogenesis of slab-derived trondhjemite–tonalite–dacite/adakite magmas. Earth Environ Sci Trans R Soc Edinb. 1996;87(1–2):205–15.

[140] Muller D, Groves DI. Tectonic settings of potassic igneous rocks. In: Potassic Igneous rocks and associated gold-copper mineralization. Cham: Springer; 2019. p. 31–71.
[141] Gorton MP, Schandl ES. From continents to island arcs: a geochemical index of tectonic setting for arc–related and within–plate felsic to intermediate volcanic rocks. Can Mineralogist. 2000;38(5):1065–73.
[142] Pearce JA, Harris HBW, Tindle AG. Trace element discrimination diagrams for the tectonic interpretation of grantic rocks. J petrology. 1984;25(4):956–83.
[143] Cheng SH, Wang Y. Geochemical modeling of Nb–Ta–La fraction in TTG suite constraints on archean plate subduction and continental crust growth. Geotectonica Et Metallogenia. 2011;35(1):95–104 (in Chinese with English abstract).
[144] Wang KB, Yang HB, Zhao BQ, Feng LI, Zhang ZY, Wang C. Sedimentary environmental analysis and basin evolution of the ancient proterozoic of gantaohe group in the mid–southern section of taihang mountain. J Hebei GEO Univ. 2018;41(3):8 (in Chinese with English abstract).
[145] Li QG, Liu SW, Wang ZQ, Zhang F, Chen YZ, Wang T. LA–ICP–MS U–Pb geochronology of the detrital zircons from the Jiangxian Group in the Zhongtiao Mountain and its tectonic significance. Acta Petrol Sin. 2008;24(6):1359–68.
[146] Li Q, Chen X, Liu S, Wang Z, Zhou Y, Zhang J, et al. Evaluating the provenance of metasedimentary rocks of the Jiangxian Group from the Zhongtiao Mountain using whole–rock geochemistry and detrital zircon Hf isotope. Acta Geol Sin. 2009;83(3):550–61.
[147] Zhang SF. Comparative study and tectonic significance of granitic rock mass in Zanhuang–Lincheng area. Hebei GEO University; 2018. p. 1–10 (in Chinese with English abstract).
[148] Ikeda Y, Yuasa M. Volcanism in nascent back–arc basins behind the Shichito Ridge and adjacent areas in the Izu–Ogasawara arc, NW Pacific evidence for mixing between E-type MORB and island arc magmas at the initiation of back–arc rifting. Contrib to Mineral Petrol. 1989;101:377–93.